Geomechanics for Energy and the Environment 39 (2024) 100581

Contents lists available at ScienceDirect

Geomechanics for Energy and the Environment

journal homepage: www.elsevier.com/locate/gete

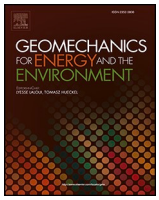

Synthesis of results for Brine Availability Test in Salt (BATS) DECOVALEX-2023 Task E

Kristopher L. Kuhlman [a,*], Jeroen Bartol [b], Steven J. Benbow [c], Michelle Bourret [d], Oliver Czaikowski [e], Eric Guiltinan [d], Kyra Jantschik [e], Richard Jayne [a], Simon Norris [f], Jonny Rutqvist [g], Hua Shao [h], Philip H. Stauffer [d], Hafssa Tounsi [g], Claire Watson [c]

[a] Sandia National Laboratories (SNL), USA
[b] Centrale Organisatie Voor Radioactief Afval (COVRA), the Netherlands
[c] Quintessa Limited, UK
[d] Los Alamos National Laboratory (LANL), USA
[e] Gesellschaft für Anlagen, und Reaktorsicherheit (GRS), Germany
[f] Nuclear Waste Services (NWS), UK
[g] Lawrence Berkeley National Laboratory (LBNL), USA
[h] Bundesanstalt für Geowissenschaften und Rohstoffe (BGR), Germany

ARTICLE INFO

Editors-in-Chief:Jens Birkholzer.

Keywords:
Salt
Brine
Thermal-hydrological-mechanical
Two-phase flow
Modeling comparison
Benchmark

ABSTRACT

In the 2023 phase of the international collaborative DECOVALEX modeling project, Task E focused on understanding thermal, hydrological, and mechanical (THM) processes related to predicting brine migration in the excavation damaged zone around a heated excavation in salt. Salt is attractive as a disposal medium for radioactive waste because it is self-healing and is essentially impermeable and non-porous in the far field. Investigation of the short-term, near-field behavior is important for radioactive waste disposal because this early period strongly controls the amount of inflowing brine. Brine leads to corrosion of waste forms and waste packages, and possible dissolution of radionuclides with brine transport being a potential transport vector to the accessible environment.The Task was divided into steps. Step 0 included matching unheated brine inflow data from boreholes at the Waste Isolation Pilot Plant (WIPP) and matching temperature observations during a Brine Availability Test in Salt (BATS) heater test. Step 1 included validation of models against a thermo-poroelastic analytical solution, and two-phase flow around an excavation. Finally, Step 2 required all the individual components covered in steps 0 and 1 to come together to match observed brine inflow behavior during the same BATS heater test.There were a range of approaches from the teams, from mechanistic to prescriptive. Given the uncertainties in the problem, some teams used one- or two-dimensional models of the processes, while other teams included more geometrical complexity in three-dimensional models. Task E was a learning experience for the teams involved, and feedback from the modeling teams has led to changes in follow-on BATS experiments at WIPP. The primary Task E lessons learned were the impact of hydrologic initialization methods (wetting up vs. drying down), the difference between confined and unconfined thermal expansion, and the large changes in permeability associated with heating and cooling.

1. Introduction

Long-term predictions of coupled thermal, mechanical, and liquid and gas transport processes around underground excavations are important for applications in disposal of radioactive waste, [22,55] hydrogen storage,[60] carbon sequestration,[8] and geothermal energy production.[44] To improve model prediction of complex coupled thermal, hydrological, mechanical, and chemical (THMC) processes requires validation of conceptual and numerical models against experimental data. The DEvelopment of COupled models and their VALidation against EXperiments (DECOVALEX) international model benchmarking program is generally interested in developing understanding and predictive simulation capabilities for coupled processes relevant to radioactive waste disposal in geologic formations.[5] DECOVALEX has been ongoing

* Corresponding author.
E-mail address: klkuhlm@sandia.gov (K.L. Kuhlman).

https://doi.org/10.1016/j.gete.2024.100581
Received 19 February 2024; Received in revised form 28 May 2024; Accepted 15 June 2024
Available online 4 August 2024

since the first round started in 1992, with the current phase (DECOVALEX-2023) being the eighth installment (2020–2023). DECOVALEX-2023 is divided into eight tasks (A through G, including F1 and F2). Task E of DECOVALEX-2023 involves comparison of models to both historical and recent data illustrating the impact of brine availability in bedded salt deposits under heated conditions associated with permanent disposal of heat-generating radioactive waste in a salt repository. Brine can impact salt repository long-term performance (e.g., DECOVALEX-2023 Task F2[38]) by corroding waste forms and waste packages and possibly mobilizing radionuclides from the repository to the biosphere via liquid-phase transport.[32] Any free brine present in the repository can also provide mechanical backpressure (i.e., it is less compressible than gas), slowing down final drift creep closure.

The DECOVALEX format involves iterative refinement and comparison of both conceptual and numerical models related to coupled processes over a 4-year cycle. The phase described here included 17 international organizations. Task E of DECOVALEX-2023 broadly included aspects of the TH^{2}M behavior (here H^1 indicates single-phase hydrological processes involving only air or brine, while H^2 denotes two-phase hydrological processes including both air and brine) of salt during heating, and more specifically the Brine Availability Test in Salt (BATS) experiment being conducted underground at the Waste Isolation Pilot Plant (WIPP).[36,35]

The 4-year investigation as part of Task E included a historic brine inflow dataset, an analytical solution, and the current BATS experiment to develop scenarios where TH^2 and TH^{2}M simulations can capture the necessary physical processes to predict brine migration in heated bedded salt formations. TH^{2}M processes are highly coupled in salt[32,49] and some key processes or the degree of coupling between processes are uncommon in other geomaterials (e.g., granitic or argillitic rocks). For example, the thermal conductivity of salt is high (about 5 W/(m·K)) and displays a strong temperature dependence.[51] The excavation damaged zone (EDZ) is relatively large and dynamic in salt, at repository-relevant depths.[18] Thermal pressurization of heated salt is another example, due to the very low hydraulic diffusivity of salt, and the pressure-sensitivity of damage-derived fractures.[39,40,45,9] This increased pressure may drive some brine away from sources of heat. Salt creeps in response to sustained deviatoric stress in both intact and granular salt backfill, with the creep closure rate being both stress and temperature dependent.[19] In addition, the heating of brine may drive evaporation and condensation of water or changes in mineral solubility which may drive dissolution and precipitation of the rock salt itself.[26,27,28]

The TH^{2}M coupled processes of interest occur in the presence of an EDZ surrounding all excavations (i.e., drifts and boreholes) in salt. The EDZ is characterized as a fractured zone with higher porosity (ϕ) and intrinsic permeability (k) than intact salt, and the EDZ porosity is filled with a mixture of both air and liquid brine ($S_e < 1$, relative liquid saturation). Material properties of the host rock change in the EDZ due to increased porosity and accumulation of plastic damage. The EDZ is surrounded by a larger excavation disturbed zone (EdZ) which has minimal damage, but still has a perturbed state (e.g., liquid pressure (p), liquid saturation, temperature (T), and mechanical stress (σ)) compared to the far field. The evolution of the EDZ and EdZ through time and space in the presence of heating and cooling (Fig. 1) is a significant complexity, which can impact brine availability.[10,18]

Each group participating in the steps (detailed in the next section) of Task E used one or more different modeling tools, summarized below.

- BGR participated in all steps using OpenGeoSys,[30] which is an open-source finite element (FE) multi-physics platform for the simulation of TH^{2}MC processes in porous and fractured media primarily developed out of the Helmholtz Centre for Environmental Research (UFZ, Germany).
- COVRA participated in steps 0a, 0b, 1a, and 1b using COMSOL Multiphysics,[7] which is a general-purpose commercial FE simulator allowing solution of a wide range of physical problems.

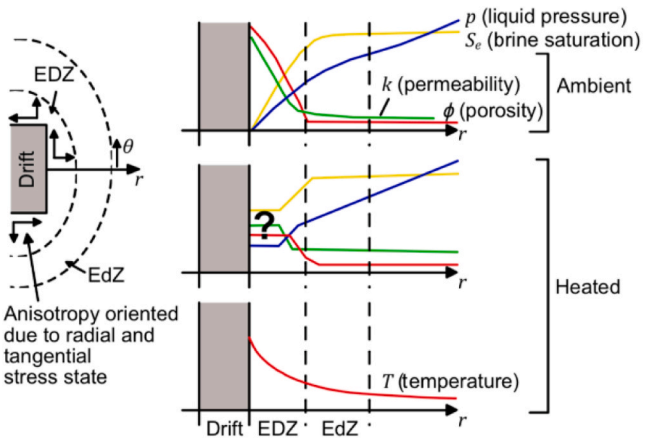

Fig. 1. Idealized 1D distributions of properties and state across the EDZ and EdZ (in radial, r, and azimuthal, θ, directions) surrounding an excavation.[33]

- GRS participated in steps 0a and 0b using CODE_BRIGHT,[43] which is a TH^{2}M FE simulator for COupled DEformation, BRIne, Gas and Heat Transport problems and was initially developed with a focus on saline media.
- LANL participated in all the steps using FEHM,[61] which is an open-source finite volume (FV) TH^{2}MC simulator developed at LANL with salt-relevant functionality.
- LBNL participated in all the steps using TOUGH-FLAC, which is an TH^{2}MC simulator[47] that links the TOUGH integrated finite differences (like FV) multiphase fluid and heat transport simulator[29] with the commercial finite difference (FD) FLAC3D geomechanical simulator[23] with salt-relevant functionality.
- SNL participated in all the steps using both PFLOTRAN and TOUGH. PFLOTRAN is a community-developed massively parallel open-source FV TH^{2}C simulator with salt-relevant functionality.[17]
- Quintessa/NWS participated in all the steps using QPAC, which is a general-purpose FV multiphysics simulator developed by Quintessa.[46]

In Task E, the teams participated in five steps (0a, 0b, 1a, 1b, and 2) that increased in complexity and realism, beginning with historical single-phase unheated brine inflow (H^1) and heat conduction (T), to coupled (TH^{2}M) brine migration from BATS. The participating teams came to the problem with a range of modeling tools and conceptual approaches, but over the four years of DECOVALEX-2023, a significant amount of learning occurred both within and between teams. Feedback and lessons learned during the modeling of BATS in DECOVALEX-2023 have also led to changes in the design of follow-on BATS experiments.

In the following sections, the details of the task plan are laid out, and a high-level summary is presented for the comparisons between the teams. This manuscript focuses on the things learned across and between teams, rather than the detailed implementation of any one team, which can be found in team-specific papers.[24,25,3,4,48,52,53,58] Previous intermediate summaries of Task E findings are found in conference papers[16,15] and in the DECOVALEX-2023 Task E Final Report.[34]

1.1. Task E approach

The Task E plan included several modeling steps that increased in complexity, beginning with uncoupled heat conduction (T) and single-phase brine transport (H^1), including a single-phase thermal-hydrological (TH^1/TH^{1}M) comparison and two-phase hydrological flow around an excavation (H^2), and ending with coupled two-phase TH^{2}M simulations. This progression allowed teams to investigate and validate different aspects of their modeling tools and conceptual models using simpler datasets. The project started with simpler steps before tackling

coupled processes and field data with more complex observed responses where the causes of differences in simulation output between the teams are harder to isolate.

There were three primary differences in how each team modeled observations:

1) choices of conceptual models, dimensionality, and physics;
2) ancillary modeling choices (i.e., time and space discretization, boundary conditions, parameterization); and
3) differences in the numerical model implementations (i.e., FV vs. FE).

For example, the availability and implementation of boundary conditions varied across dimensionality and model implementations, requiring some teams to make modifications to the conceptual models. To reduce the differences associated with modeling choices, during online meetings the teams arrived at a consensus on how to simulate the system, rather than allowing too much freedom to each team. It is desirable to ensure compatible conceptual models are used for benchmarking, to reduce unnecessary differences and improve direct comparison. At the same time, it can be desirable to explore the effect different conceptual models have when interpreting experimental data, since the relevant physics or effective dimensionality of the problem is not known a priori. During initial model development each team has been allowed to develop their models independently and then to refine their models and learn from each other, finally agreeing upon a particular common method for benchmarking.

Task E of DECOVALEX was organized into five "steps" beginning with step 0a.[33] Step 0a focused on uncoupled single-process single-phase hydrological (H^1) and step 0b included thermal (T) modeling benchmarks. Step 1a focused on single-phase thermal-hydrological (TH^1) or thermal-hydrological-mechanical (TH^1M) and step 1b included multi-phase hydrological (H^2) modeling. Step 2 finally brought together aspects from steps 0a, 0b, 1a, and 1b with the application of TH^2M models to simulate brine inflows from the BATS experiment. The steps are laid out below in more detail.

Step 0: Single-process H^1 and T benchmarks.

- **Step 0a**: Simulate single-phase brine production into three boreholes in salt using ambient temperature brine inflow data from the WIPP small-scale brine inflow test.[12]
- **Step 0b**: Simulate the temperature distribution due to solid-phase heat conduction from a constant-temperature borehole heat source for five thermocouple locations during the January to March 2020 BATS heating and cooling cycle.[36] Teams were provided with temperature data through time, laboratory estimates of thermal properties, and relevant coordinates and distances between the source and measurement points.

Step 1: TH^1M benchmarking and H^2M/H^2 unheated drift dry-out.

- **Step 1a**: Benchmark against a thermo-poroelastic analytical solution for TH^1M brine production to a heated borehole, matching the solution of McTigue[40] along space and time profiles, using properties given for salt in Table 1 of McTigue.[39]
- **Step 1b**: Simulate H^2M/H^2 brine production into an excavation under multi-phase ambient conditions, predicting gradients in fluid pressure and brine saturation across the EDZ. The output from these H^2M/H^2 simulations become the initial conditions for the TH^2M heated BATS test case (step 2). Few two-phase flow data exist for a fractured-salt EDZ, so data came from literature surveys including using analogous non-halite WIPP rocks or oilfield rocks with existing data.[21,11]

Step 2: TH^2M multi-phase brine inflow through a heated EDZ during a heater tests (BATS)

- **Step 2**: Simulate brine production into a borehole in salt under multi-phase heated conditions (including production changes at the onset of heating and cooling), building on previous steps. Brine production data from the heated BATS array through time were provided, including after turning off the heater. The effects of thermal expansion on the stress, ϕ, and k of the salt (i.e., closing and opening of EDZ microfractures) were included in models.

Several possible extensions were proposed initially as a "Step 3" in the initial task specification,[33] but these were not completed during DECOVALEX 2023. The following sections go into the details of each step.

2. Step 0a: unheated single-phase brine inflow

Finley et al.[12] reported brine production from boreholes as part of the "small-scale brine inflow" experiments at WIPP. These experiments monitored brine production to 17 unheated boreholes, that was the focus of the previous INTRAVAL model validation exercise.[2]

For Task E the teams focused on three boreholes (L4B01, DBT10 and DBT11; Fig. 2). L4B01 is a 10 cm diameter horizontal borehole completed in the argillaceous halite of Map Unit 0 (MU-0) in Room L4. DBT10 and DBT11 are part of an array of vertical boreholes (DBT10 through DBT13) drilled into the floor of Room D approximately 3.5 years after the room was excavated. The lines plotted with the data in Fig. 2 have slightly different best-fit parameters for each borehole (see Tables 4–4 of Beauheim et al.[2] derived from McTigue[41]). These boreholes spanned several map units, including a disseminated clay-rich layer (Clay F) between Map Units 4 and 5 (Fig. 3). These boreholes show characteristic exponential decay of brine inflow with time.

2.1. Brine production results

2.1.1. Horizontal borehole L4B01

Horizontal borehole L4B01 is entirely contained within a single stratigraphic unit (MU-0) giving it the simplest geometry and stratigraphy. Each team constructed their models using 1D or 2D radially symmetric geometries (Fig. 4). LANL, Quintessa, and BGR explicitly included a borehole EDZ as a high-permeability region surrounding the borehole while LBNL and COVRA neglected it. LANL and LBNL performed variably saturated (H^2) flow simulations, while other hydrological simulations were single-phase (H^1). LANL also included the effects of the access drift on the initial pressure and saturation profile.

Table 1
Step 0a: Model Implementations for Room D benchmarking.

Team	Dim.	Bore EDZ	Drift EDZ	Map units	Domain size (m)	Far field pressure (MPa)	Perm.
BGR	2D	Yes	No	Yes	80	10	layers
COVRA	2D & 3D	No	No	No	0.5–6	2–16	uniform
GRS	2D	No	No	Yes	8	12	layers
LBNL	3D	No	No	Yes	$5 \times 10 \times 40$	8–12	layers
SNL	3D	Yes	Yes	Yes	$5 \times 10 \times 40$	12	layers
LANL	3D	Yes	Yes	Yes	$10 \times 30 \times 40$	12	layers
Quintessa/NWS	1.5 D	Yes	No	Yes	12	9–15	layers $k(r)$

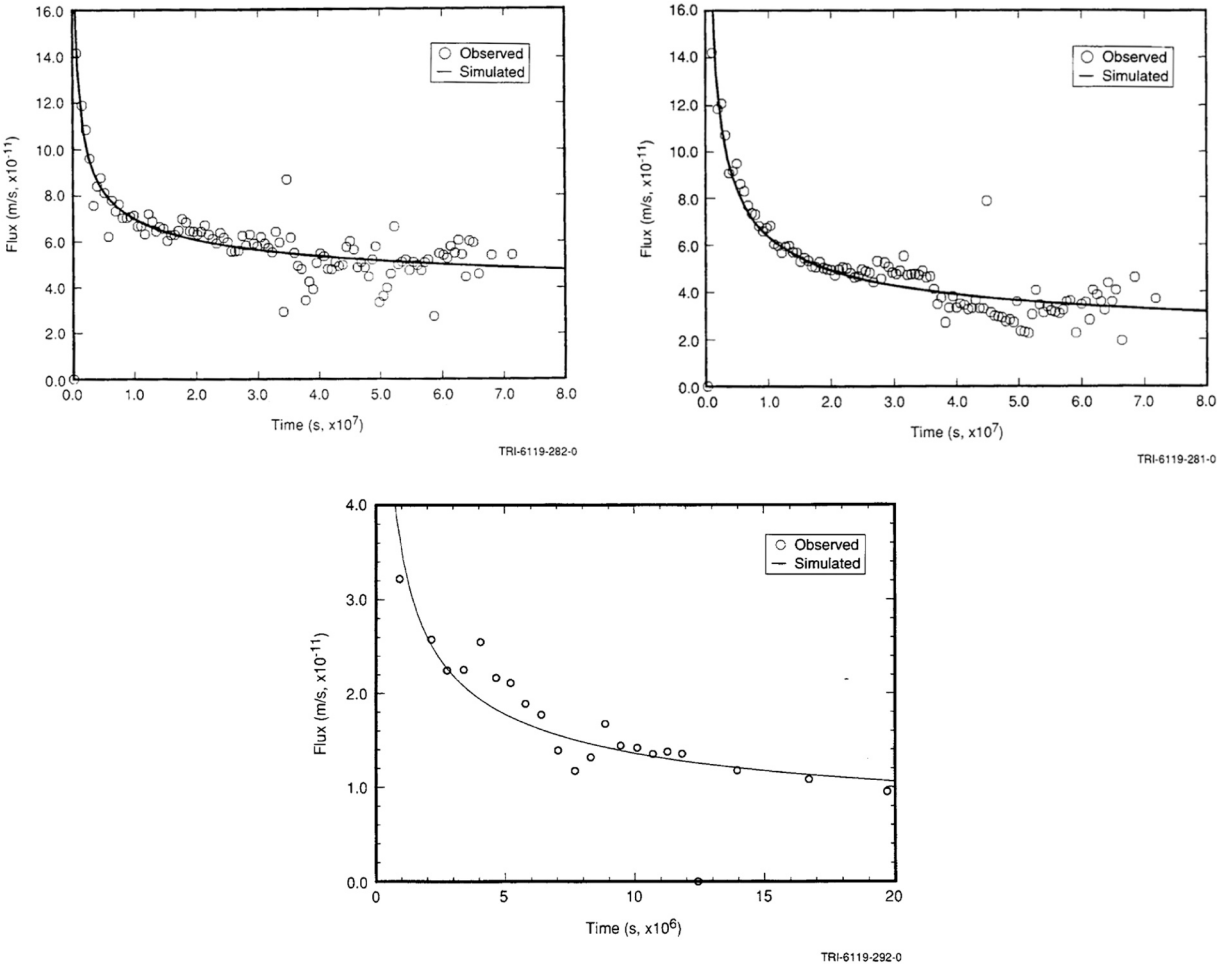

Fig. 2. Unheated small-scale brine inflow results, with per-borehole fits to analytical solutions as part of INTRAVAL.[2] Vertical boreholes DBT10 (upper left) and DBT11 (upper right) intersected Clay F, while horizontal borehole L4B01 (lower) is completed in argillaceous halite, MU-0.

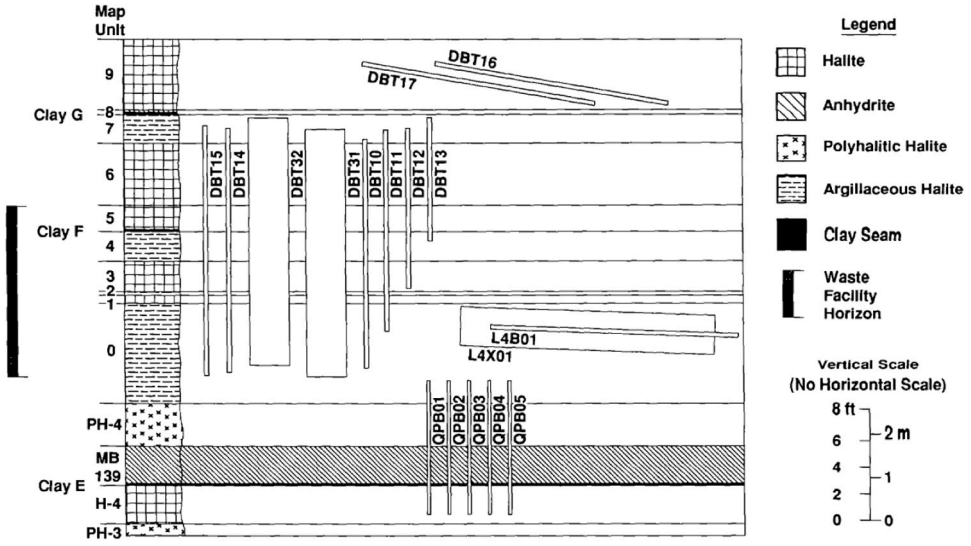

Fig. 3. Generalized WIPP stratigraphy and relative orientation of boreholes used in small-scale brine inflow test.[12]

Despite these conceptual model differences, the results of each team were in relatively close agreement with each other and the observations (Fig. 5).

Most of the models match the late-time data better than the early-time data (<300 days), and there is general agreement between model predictions.

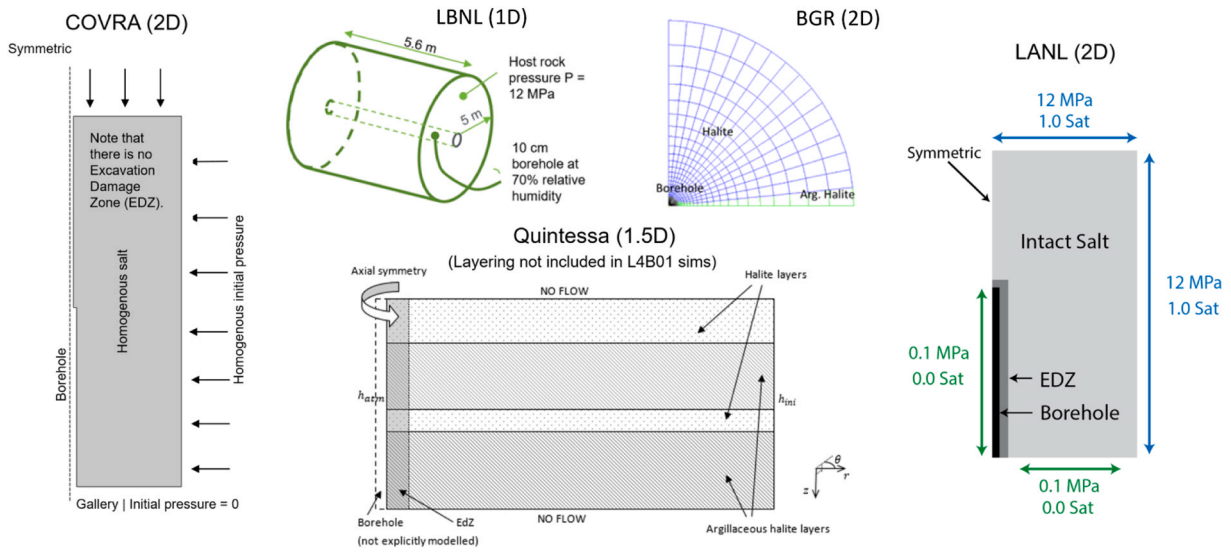

Fig. 4. Step 0a: conceptual models used for L4B01. Quintessa model is 2D without vertical connections (i.e., 1.5D) and used a single unlayered lithology for L4B01.

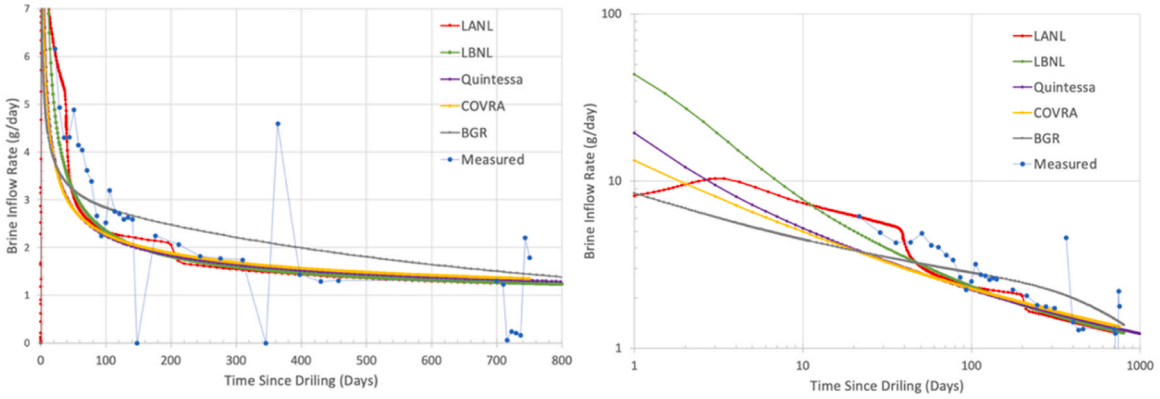

Fig. 5. Step 0a: L4B01 brine inflow predictions (heavier lines and small symbols) and data (thin line and larger blue symbols); left subplot is linear, right subplot is same results on log scale.

2.1.2. *Vertical boreholes DBT10 and DBT11*

The Room D boreholes have a more complex configuration due to the crossing lithologic layers within the halite and the potential influence of multiple adjacent boreholes. Each team was free to develop their own conceptual model of the experiment (Fig. 6). Some models included the layering while others approximated the lithology with a subset of the

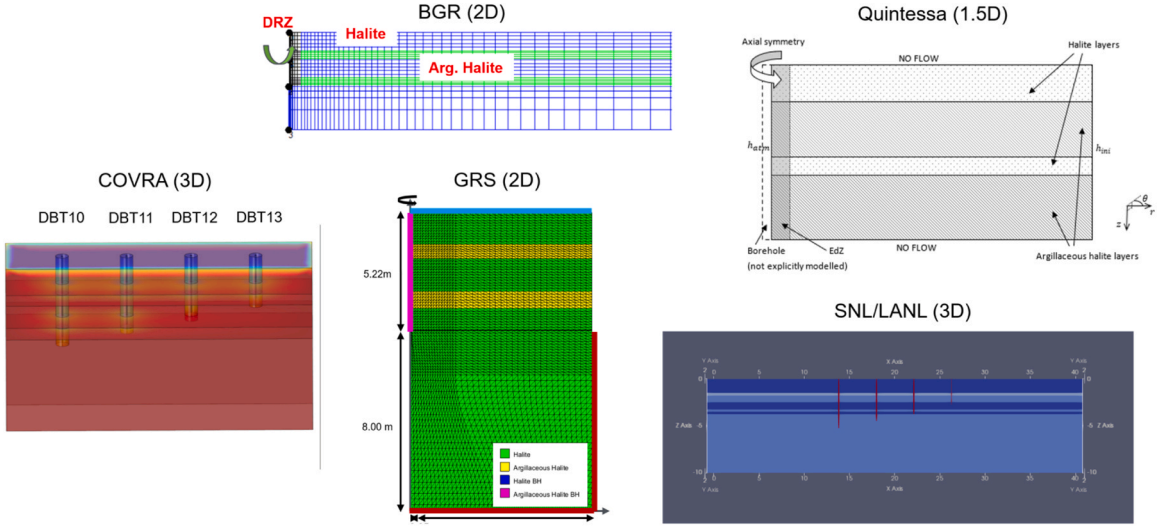

Fig. 6. Step 0a: Conceptual Models used for Vertical Room D boreholes.

units. Likewise, some included all the boreholes in the array (DBT10-DBT13) while others simplified it to only one borehole. Despite these differences there was good agreement between each modeling team demonstrating that the lithology can likely be simplified into a homogeneous unit, from the point of view of matching pressure-driven brine inflow data. The predictive capability of homogenized models may not be as good as those with explicit stratigraphy included. Table 1 includes a summary of the different characteristics of each of the conceptual models shown in Fig. 6.

The brine production predicted with LANL's 3D model deviated the most from the other models in boreholes DBT10 (Fig. 7), and both the LANL models produced significantly different results for DBT11 (Fig. 8). These differences are at least partly due to how the teams implemented the EDZ associated with the access drifts and their associated boundary and initial conditions.

In both DBT10 and DBT11, a late time increase in brine production was observed (>900 days). This was also observed in other boreholes in the INTRAVAL exercise. [2] This late-time increase cannot be re-created in models that have constant model properties and drive flow down a pressure gradient (i.e., exponential decay of brine inflow rate), therefore most of the teams did not attempt to model this portion of the data. This late-time increase may be due to an increasing EDZ with time (i.e., mechanical effects), as found in sensitivity investigations by Webb.[59] BGR used a model that considered the EDZ growth through time (Fig. 9), achieved by using the restarting capability of OpenGeoSys; the simulation was continued at approximately 810 days with increased permeability, leading to increased brine inflow rate.

3. Step 0b: BATS heat conduction

The BATS experiment is a series of borehole-based experiments conducted underground at WIPP.[36,35] The as-built experimental setup is presented in Kuhlman et al.,[36] which includes the drilling and instrumentation of two arrays of 14 horizontal boreholes, completed mostly in the clean halite layer MU-3 (Fig. 3). One array includes a central heated borehole while the unheated array serves as an unheated control. Each array includes a central borehole (HP) with a heater (in the heated array only) behind an inflatable packer, with dry N_2 gas circulation used to remove brine (Fig. 10). Surrounding the central borehole are parallel boreholes for temperature sensors only (T), acoustic emissions (AE), a cement seal (SL), tracer injection (D), electrical resistivity tomography (E), fiber optic monitoring (F), and liquid brine sampling (SM). Guiltinan et al.[14] showed the results of modeling the initial "shakedown" phases of BATS. This effort refined the BATS experiments that appear in DECOVALEX-2023. Geophysical data from BATS1, that show evidence for migration of brine due to thermal pressurization, are discussed in Wang et al.[57]

The observed temperature response averaged every 15 min to the heating episode referred to as BATS 1a (January to March 2020) was used for step 0b.

Each team was asked to investigate the data as a heat conduction problem in salt. The conceptual models employed by the different teams are shown in Fig. 11.

3.1. Heat conduction results

The models used by teams varied in terms of the domain dimensionality, domain size, whether the thermal conductivity (κ_T) was a constant or a function of temperature, whether the medium was purely solid (or if the medium is porous with a fluid phase), and if an EDZ was included due to the boreholes or access drift.

Table 2 summarizes conceptual models and Fig. 12 shows the results of all the simulations compared to observations. The temperature changes due to heat conduction through solid salt was accurately simulated by all teams; all results compare well to one another and the data (black dots, which appear in places as a line due to their high frequency).

To accurately simulate the temperature response, teams either adjusted the laboratory-derived thermal conductivity and/or decreased the reported heater power input to the salt. In addition, several teams noticed slight adjustments in thermocouple locations allowed for improved ability to reproduce the observed temperatures. For example, Quintessa estimated the heater to be 91% percent efficient, and that a single thermocouple (HF1TC1) needed to be moved 3 cm to provide the most accurate result. LANL also reduced their heater efficiency to 85%, and COVRA noted a different temperature sensor than Quintessa as being possibly slightly out of position. Overall, the proposed temperature sensor movements, adjustments to the heater output, and changes to the thermal conductivity are all physically realistic.

4. Step 1a: thermal pressurization around a heated borehole

While Step 0 focused on uncoupled H[1] and T problems, Step 1 began the comparison of coupled processes via a 1D analytical thermo-poroelasticity solution from McTigue.[40] This benchmark investigated the thermal pressurization response of a heated borehole without a regional pressure gradient from the far-field to the borehole, as there was for the data interpreted in Step 0a. The analytical solution presented by McTigue[40] was compared to model results using the salt material properties given in McTigue.[39] Matching the analytical solution required disabling some non-linear constitutive laws, such as temperature-dependent fluid density, fluid viscosity, or bulk thermal conductivity. The conceptual models used by teams were divided into two groups (confined and unconfined – explained more in the next

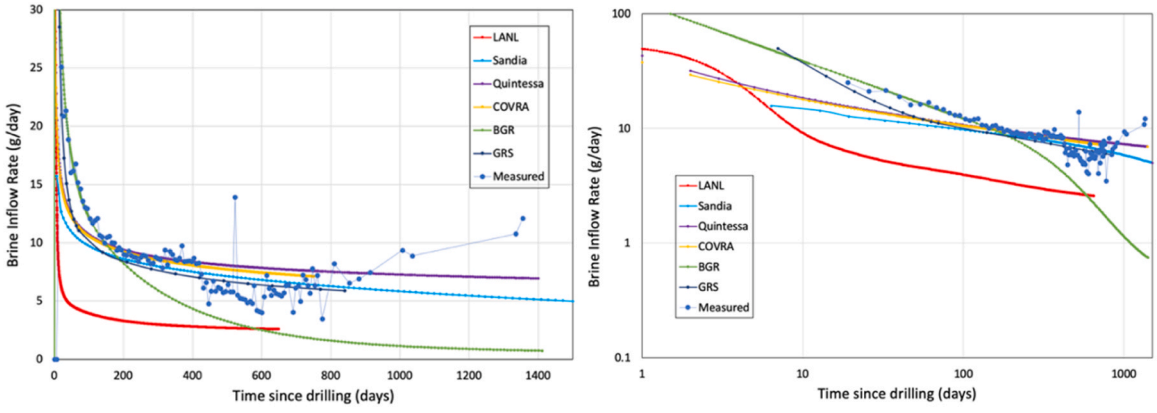

Fig. 7. Step 0a: DBT10 brine inflow predictions (heavier lines and small symbols) and data (thin line and larger blue symbols); left subplot is linear, right subplot is same results on log scale.

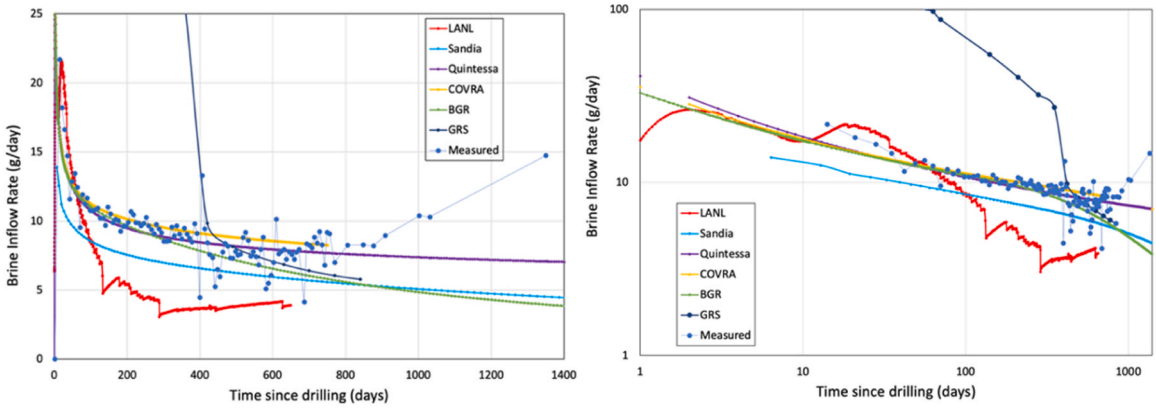

Fig. 8. Step 0a: DBT11 brine inflow predictions (heavier lines and small symbols) and data (thin line and larger blue symbols); left subplot is linear, right subplot is same results on log scale.

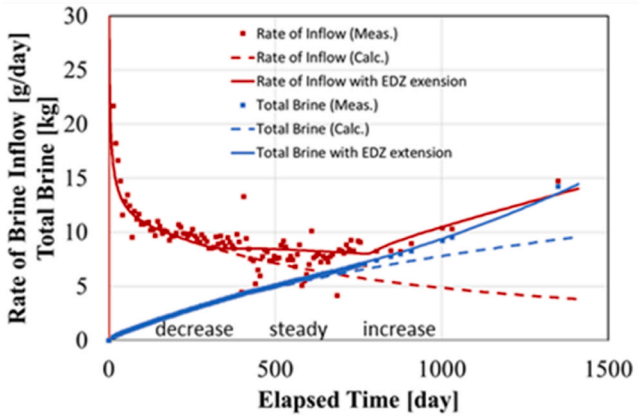

Fig. 9. Step 0a: BGR model (lines) showing increasing brine inflow in DBT11 with model predictions matching observation (square symbols) using an increasing EDZ through time.

paragraph) and the dimensionality of implementations varied between teams (Fig. 13). Some teams chose one-dimensional representations, while others chose two or three-dimensional domains. GRS did not participate in step 1a.

4.1. Pressure and brine production results

The effect of thermal expansion on the fluid pressure and borehole brine inflow rate were investigated using both TH[1] simulations and TH[1]M simulations. The TH[1]M (i.e., confined) solution considered thermal expansion of both the liquid and solid phases, which included the effects of the mechanical confinement of the surrounding solid phase. The TH[1] (i.e., unconfined) solution considered thermal expansion of only the liquid phase, assuming the solid phase either did not expand or was unconfined and therefore free to expand. Several teams investigated both approaches (Table 3).

For the parameters given in McTigue,[39] the confined response due to heating results in a thermal expansion response approximately 40 times larger than the unconfined response. The difference is largely the result of the definition of the effective thermal expansion coefficient, b'. McTigue[39] gives the one-dimensional governing equation for pressure with a thermal source term to be

$$\frac{\partial p}{\partial t} - c\frac{\partial^2 p}{\partial x^2} = b'\frac{\partial \theta}{\partial t}, \tag{1}$$

where p is fluid pressure change [Pa], θ is temperature change [K], c is fluid diffusivity [m^2/s], and b' is the thermal expansion coupling coefficient [Pa/K]. The definition of b' relevant to the confined response (Equation 27 of McTigue[39]) is

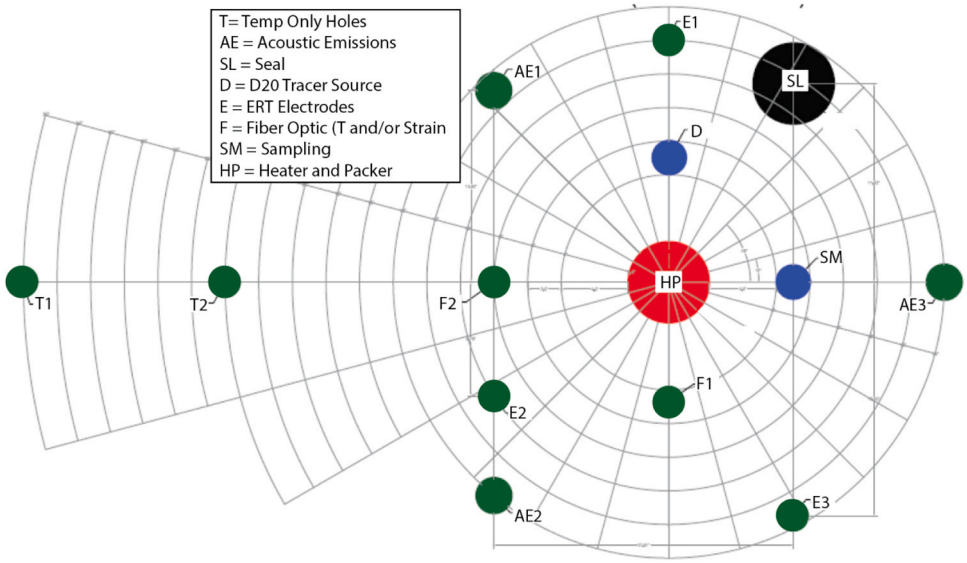

Fig. 10. Borehole layout for BATS 1a heated array.

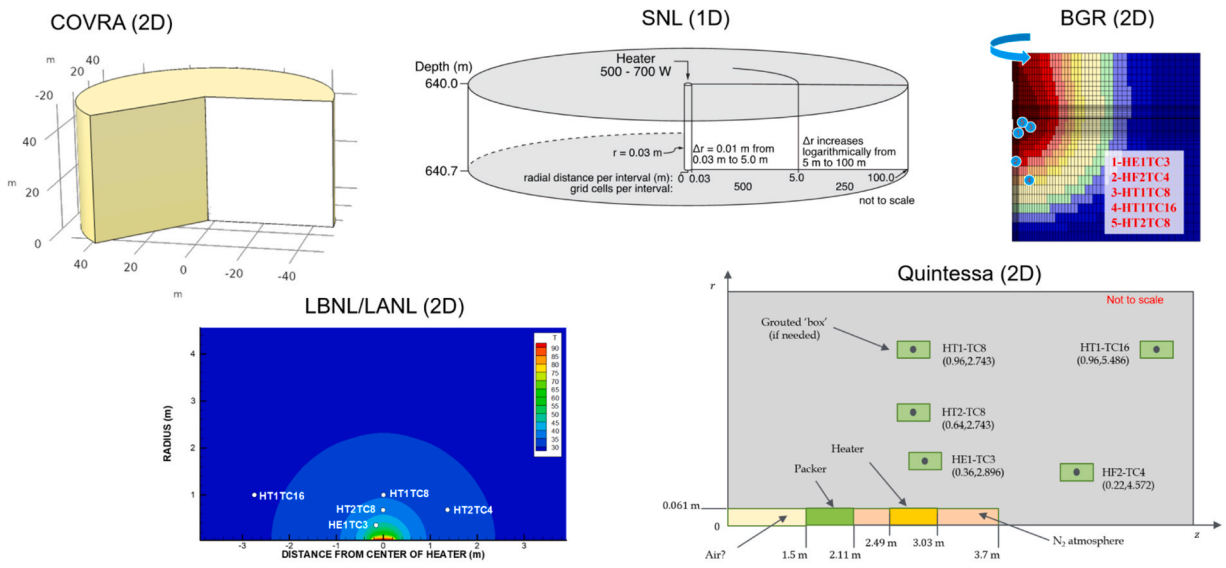

Fig. 11. Step 0b: Conceptual models used for BATS 1a heat conduction. BGR, LBNL/LANL, and Quintessa subplots also show observation locations. LBNL/LANL and BGR subplots include characteristic temperature results as color scale (red hotter, blue cooler).

Table 2
Step 0b: Team-specific modeling parameters for BATS 1a heater test.

Team	Dim.	Liquid Phase	Borehole EDZ	Drift EDZ	$k_T(T)$	Domain size (m)
BGR	2D	Yes	Yes	No	No	80
COVRA	2D (+3D)	No	No	No	Yes	50
LBNL	2D	Yes	No	No	No	5
LANL	2D	Yes	No	No	No	5
SNL	1D	Yes	Yes	Yes	No	100
Quintessa/ NWS	2D	No	No	No	Yes	10

$$b' = \frac{4GB(1+\nu_u)}{9(1-\nu_u)}\left[\alpha_s + \frac{B(1-\nu)(1+\nu_u)}{2(\nu_u-\nu)}\phi_0(\alpha_f-\alpha_s)\right], \quad (2)$$

where $G = 12.4$GPa is the shear modulus, $B = 0.93$ is the Skempton coefficient, $\nu = 0.25$ is the Poisson ratio, $\nu_u = 0.27$ is the undrained Poisson ratio, $\alpha_s = 1.2 \times 10^{-4}$ 1/K is the solid expansivity, and $\alpha_f = 3.0 \times 10^{-4}$ 1/K is the fluid expansivity.

The value for b' listed in Table 1 of McTigue[39] is 29.0 kPa/K, while a value of 1105.5 kPa/K is computed from the values listed above (also from Table 1 of McTigue). The smaller value of b' was reported to arise from $b_0' = \phi_0(\alpha_f - \alpha_s)/D$, where $D = \frac{\phi_0}{K_f} - \frac{\phi_0}{K_s} + \frac{1}{K} - \frac{1}{K_s}$ is an effective compressibility [1/Pa], $K = 20.7$ GPa is the drained bulk modulus, $K_f = 2.0$ GPa is the fluid bulk modulus, and $K_s = 23.5$ GPa is the solid bulk modulus. This simpler representation is equivalent to only keeping the second term in brackets of McTigue's Equation 27, which is negligible compared to the first term. The difference of 38.1 between these two coefficients represents the difference between the unconfined (smaller b') and the confined (larger b') models. McTigue's Table 1 reported a small value of b', consistent with the unconfined conceptual model (despite the description of the confined model in the text), because this value and conceptual model better fit data from the Salt Block II laboratory heater test[20,54] where unconfined conditions were more appropriate. This difference in reported values illustrates how the analytical solution could be matched against either the confined or unconfined numerical approaches by altering the effective thermal expansion coupling coefficient.

This benchmark included mechanical coupling, so some teams investigated the problem using different simulators than used in Step 0. LBNL utilized both COMSOL and TOUGH3 while SNL utilized TOUGH2 and PFLOTRAN. The predicted spatial profiles of brine pressure and time series of brine inflow to the central borehole for the unconfined (TH[1]) models are presented in Fig. 14, while the predicted pressure and brine inflow for the confined (TH[1]M) models are in Fig. 15.

The agreement between the teams and the unconfined analytical pressure response (Fig. 14) is considered satisfactory, although two predictions (SNL TOUGH2 and BGR) show about half as much brine flux, compared to the analytical solution. The difference is largest at early time, so it may be related to fluid and formation compressibility. For the confined pressure response (Fig. 15) BGR, LBNL, and Quintessa appear very close to the McTigue pressure response while LANL appears shifted radially and COVRA has pressures that are too high. The origin of the difference between the COVRA confined results and the other teams was not isolated (the thermal predictions for all teams were almost identical), but it is likely a parameterization or equation of state issue. The brine production values from all teams are quite similar and much higher than the unconfined case.

This McTigue solution and the TH[1]M vs. TH[1] numerical responses illustrate the coupling of TH[1]M processes during the heating of borehole in a salt formation. The benchmark produces a very high thermal pressurization response; higher than the lithostatic stress at the WIPP repository horizon of 650 m depth. Exceeding the minimum principal stress will result in hydrofracture and subsequent bleed-off of excess pressure, so this prediction of fluid pressure from thermal expansion is physically unrealistic. In salt the far-field stress state is believed to be isotropic (i.e., all 3 principal stresses being equal because salt cannot maintain deviatoric stress long-term without creeping), so the least principal stress in salt should be equal to the lithostatic stress (approximately 15 MPa at WIPP[1]).

5. Step 1b: two-phase flow to a drift through an EDZ

Step 1b is a 1D simulation of H[2] flow around a 5-m diameter drift (i.e., mined opening) without mechanical considerations. Each of the participating teams completed a simulation assuming an initially saturated 2.5 m EDZ around a 5-m diameter drift, which were both surrounded by intact salt (GRS did not participate in step 1b). Due to the lack of directly applicable two-phase flow data for fractured (i.e., EDZ) salt, a combination of data from WIPP fractured anhydrite,[21] and granular salt[42,6] are used. The absolute permeability of the intact salt and EDZ are assumed to be 10^{-21} m^2 and 10^{-17} m^2 respectively. The van

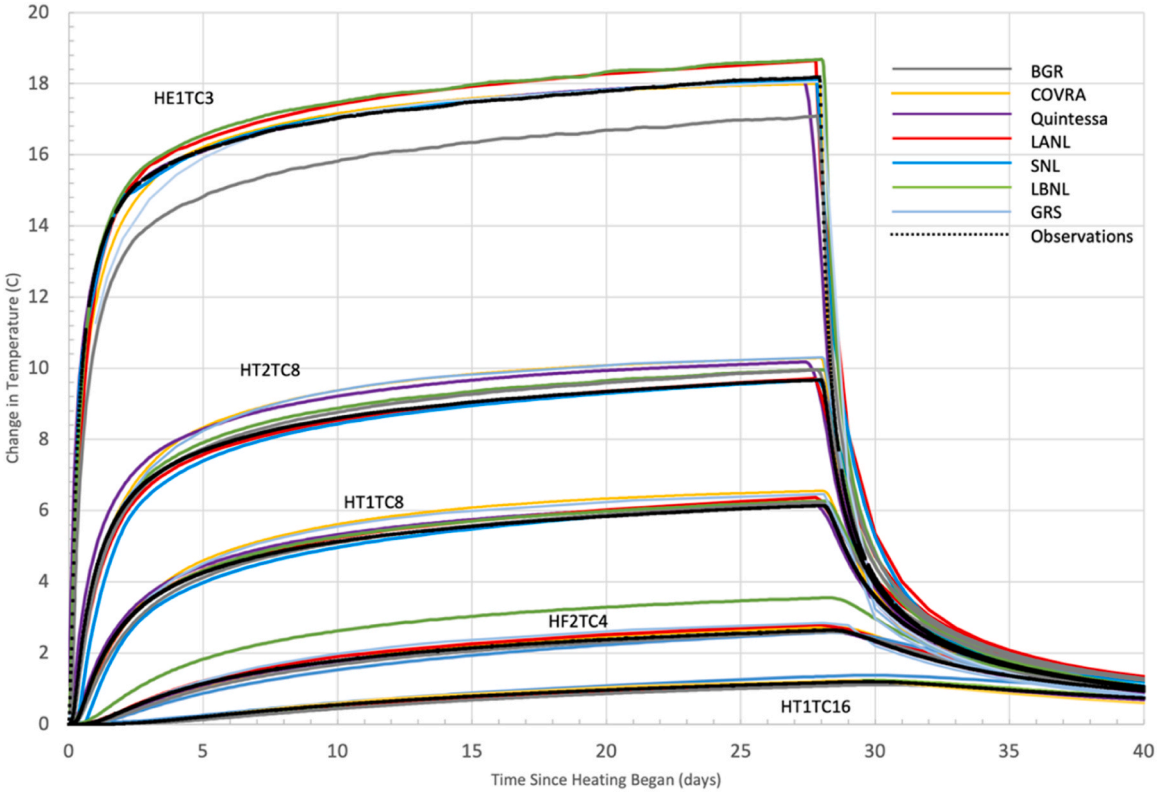

Fig. 12. Step 0b: Comparison of model predictions (colored lines) to 15-minute averages of BATS 1a temperature observations (black symbols).

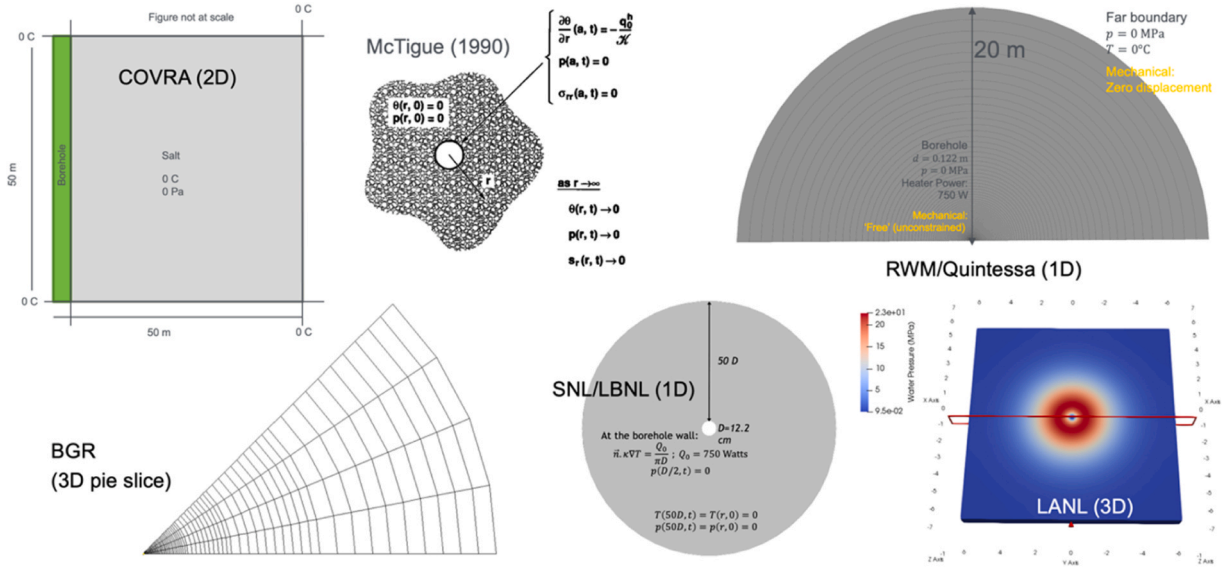

Fig. 13. Step 1a: Conceptual models for the McTigue[40] single-phase brine production to a heated borehole benchmark.

Genuchten[56] relative permeability model used an m-value (i.e., the shape factor) of 0.6, residual liquid saturation of 0.19, and entry pressures of 1.54 MPa for the intact salt and 0.0154 MPa for the EDZ. The air-entry pressure and permeability of many rocks are inversely correlated.[11] The porosity of the intact salt is set to 0.001 and the EDZ porosity is 0.01. The far-field fluid is assumed to be 12 MPa fluid pressure and completely brine saturated; the drift is filled with air at atmospheric pressure. Despite the lack of good field or laboratory data to parameterize the two-phase flow properties of the models, a set of parameters were agreed upon by the teams to reduce differences solely due to parameter choice. Because of the more prescriptive nature of this modeling exercise, the conceptual models used by teams are more similar than previous steps (Fig. 16).

5.1. Pressure and saturation results

The results are summarized in Fig. 17 as profiles at different times and brine inflow to the drift through time. The pressure profiles show a significant amount of variation at 1 h, but by 1 month all team's simulations are more similar. The saturation profiles are very similar at one

Table 3
Step 1a: Team-specific configurations for[40] solution.

Team	Dim.	TH^1/ TH^{1}M	Simulator (s)	Domain size (m)
BGR	3D slice	TH^1 and TH^{1}M	OpenGeoSys	20
COVRA	2D	TH^1 and TH^{1}M	COMSOL	50
LANL	3D box	TH^{1}M	FEHM	6.1–8.6
SNL	1D	TH^1	TOUGH2 or PFLOTRAN	6.1
LBNL	1D	TH^1 and TH^{1}M	COMSOL + TOUGH3	6.1
Quintessa/ NWS	1D	TH^1 and TH^{1}M	QPAC	20

hour because the entire domain is mostly saturated, but by 10 years some differences are noted. All simulations used the agreed upon "drying down" conceptual model and therefore even after 10 years the intact salt adjacent to the EDZ remains fully saturated. In the drying down conceptualization, the intact salt and EDZ begin at full saturation and higher-pressure brine initially located in the EDZ flows quickly to the low-pressure boundary condition in the excavation.

There was no consensus on brine inflow prediction, with predictions ranging from approximately 25 to 225 kg. It is notable that even when using a more prescriptive conceptual model, teams produced different estimates for the total brine flow. This provides some insight into the difficulties of multiphase flow benchmarks. These differences are partially due to ancillary differences (e.g., time stepping, spatial gridding, boundary condition implementation) and the differences in implementation between modeling tools. The largest differences between models were the treatment of the drift boundary condition and pore compressibility, which have more impact at early time and near the drift

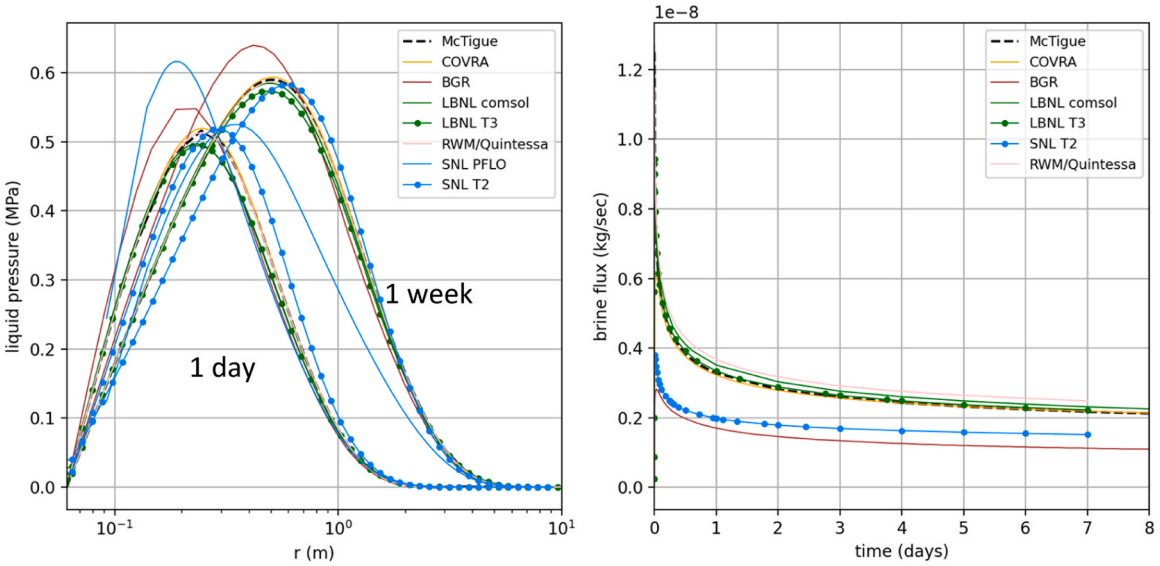

Fig. 14. Step 1a: TH1 (i.e., unconfined) numerical simulation vs. analytical solution (black dashed line). Liquid pressure after 1 day and 1 week of heating (left) and brine flux to the borehole through time (right).

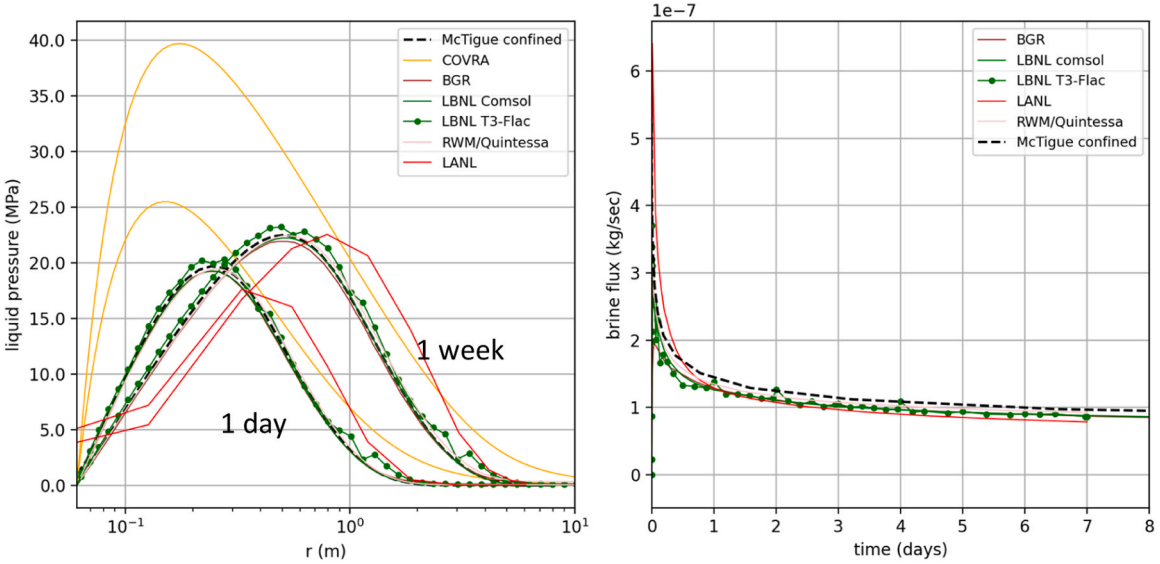

Fig. 15. Step 1a: TH^{1}M (i.e., confined) numerical simulation vs. analytical solution (black dashed line). Liquid pressure at 1 day and 1 week of heating (left) and brine flux to the borehole through time (right).

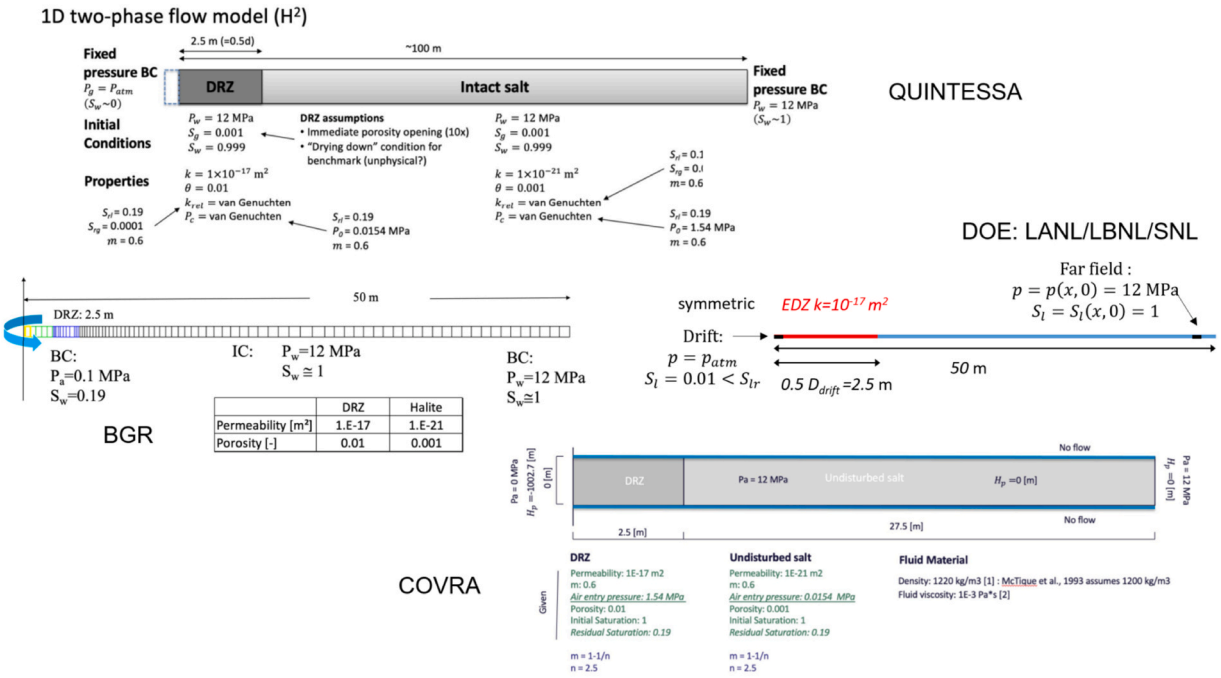

Fig. 16. Step 1b: Conceptual models for the 1D H^2 modeling exercise.

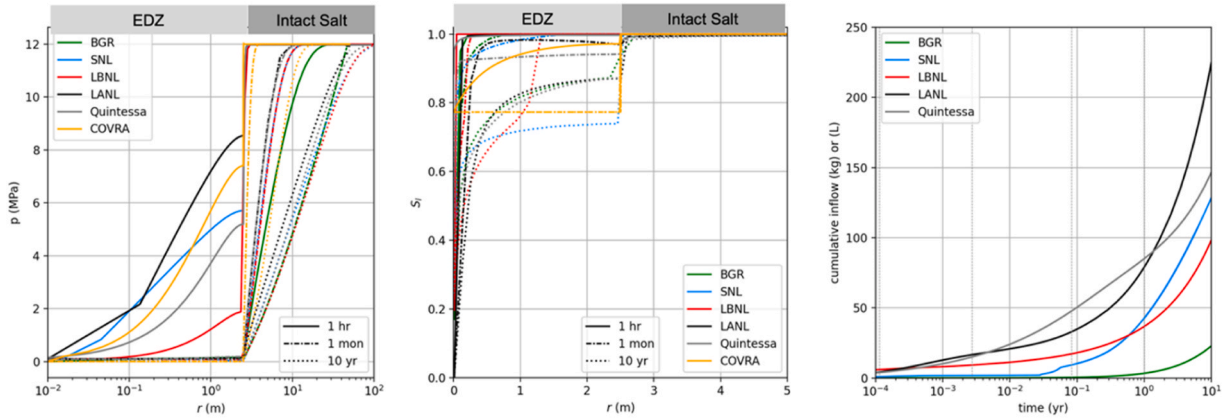

Fig. 17. Step 1b: Results of the 1D H^2 model exercise at 1 h, 1 month, and 10 years for pressure (left) and saturation (middle). Line color indicates team, line style (solid, dashed, dotted) indicates time. Cumulative brine inflow predicted to the drift (right).

face (especially visible in log-scaled left and right panels of Fig. 17).

This modeling exercise did not have a direct set of observations for benchmarking against. It is difficult to make measurements of brine production to rooms because the brine is mostly lost to evaporation into the mine ventilation or it is lost into fractures in the EDZ.[13] BGR showed the predicted brine inflow rates are analogous to those scaled up from the borehole tests reported in Step 0a (Fig. 18). This indirect comparison shows the drift-scale results are likely in the right order of magnitude, assuming the drift can be treated like a scaled-up (i.e., 5-m diameter) borehole.

During this modeling exercise, teams agreed to assume the EDZ started completely liquid saturated (numerically simpler to setup and simulate than starting out air-filled), with a Dirichlet boundary condition of atmospheric-pressure gas at the drift. Quintessa illustrated the difference in response associated with changing the initial conceptualization. An alternative to the "drying down" approach adopted by the step 1b modeling exercise was a "wetting up" conceptualization, which starts off at low liquid saturation and brine slowly flows in from the far field to wet it back up (Fig. 19). The wetting-up conceptualization

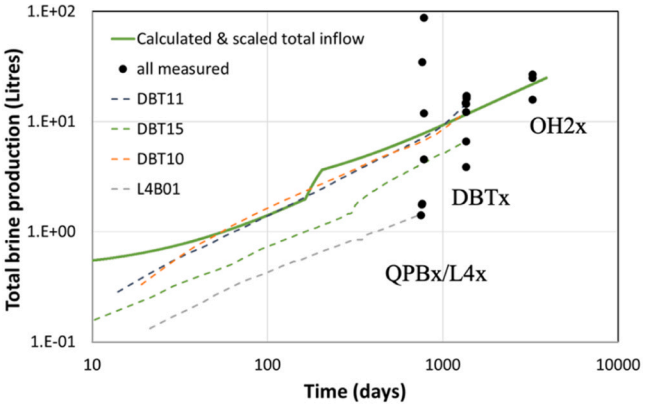

Fig. 18. Step 1b: Comparison between model-predicted brine production from drift (green solid line) and scaled-up boreholes models (dashed lines) from Step 0a and observations (black filled circles).

contends that a 10 × increase in EDZ porosity simultaneously leads to a 10 × reduction in liquid saturation (i.e., no new brine flows into the EDZ during damage accumulation). In the drift EDZ, damage porosity is rapidly created due to lack of confinement and increased deviatoric stress (radial stress goes to zero, so circumferential stress must increase). This damage-induced porosity forms quickly and the far-field permeability is low. This arrangement does not allow for brine to flow in fast enough from the far field to keep the EDZ fully saturated with brine.[31]

The "drying down" conceptualization is a simpler initial condition to initialize in an H^2 model, and the simulation runs faster to completion, but it is an inaccurate representation of field conditions in the underground at WIPP. This conceptualization creates 100 × more brine inflow in 10 years than the "wetting up" scenario (Fig. 19, third column of subplots), and results in a very large initial peak of brine production at early time (which is not observed in the field[13]). The results in Fig. 19 also show the impact that two-phase flow parameters have on model predictions is small compared to the difference in the initialization. The top two rows represent properties taken from Olivella et al.[42] for granular salt and Howarth & Christian-Frear[21] for fractured WIPP anhydrite. This demonstrates the relative impact of two-phase parameter variability compared to the impact of the initial conditions on apparent model-predicted brine availability and shows some initializations of H^2 models produce physically unrealistic results.

These two conceptualizations are not the only options; they represent end members. The real initial condition may lie between them. It is possible that some brine does flow in to fill some of the new porosity. It is also possible that some newly created porosity is air-filled, but it is also un-connected from the overall flow network and therefore does not contribute to flow.

The two conceptualizations will likely reach similar steady-states, but it can take a long time due to the low permeabilities of the porous media. Fig. 19 shows that after 100 years, the pore pressure and brine flux are approaching similar values across all three cases, but they are not yet identical and at 100 years the brine saturation remains quite different across the EDZ. If the output of this simulation is only used as the input for a second simulation (e.g., the initial condition for a long-term performance assessment calculation), the distributions will be similar, but the difference is much larger at early time (i.e., <10 years), and may take thousands of years to reach a true equilibrium, for the parameters chosen here.

6. Step 2: BATS brine inflow prediction

The third step (Step 2) combined individual processes included in steps 0a, 0b, 1a and 1b, discussed in the previous sections. This final step involved simulating observed brine inflow data from the BATS 1a heater test.[36,35] Brine production is strongly influenced by the salt temperature during heating, which was already simulated during step 0b (Section 2). The migration of brine towards the borehole included aspects of the single-phase isothermal brine inflow down a pressure gradient from step 0a (Section 0) and two-phase initial condition developed for a ventilated drift in step 1b (Section 4). The differential thermal expansion of brine and salt, considered for step 1a (Section 3), contributes to driving flow towards the borehole in the BATS 1a test.

For step 2, the teams focused on predicting radial profiles of fluid pressure and brine saturation going away from the heated borehole. These profiles were reported during and immediately after heating. The teams also predicted a time series of brine production into the heated HP borehole. Only brine production data were provided from the BATS experiment; no observations of liquid pressure or saturation in the formation were made.

The teams used a variety of conceptual and numerical models to implement step 2 (Table 4), with most of the approaches being an extension or modification of approaches used in earlier steps. The GRS and COVRA teams did not participate in step 2. The largest difference between the models used for previous steps and those used for step 2 was modifying permeability associated with the heating and cooling during the BATS 1a heater test.

Quintessa used a one-dimensional conceptualization, while BGR, LBNL, and LANL used two-dimensional conceptualizations of the heater test. Both SNL and LANL used 3D conceptualizations (Fig. 20). Given the existence of multiple EDZs associated with the horizontal heated

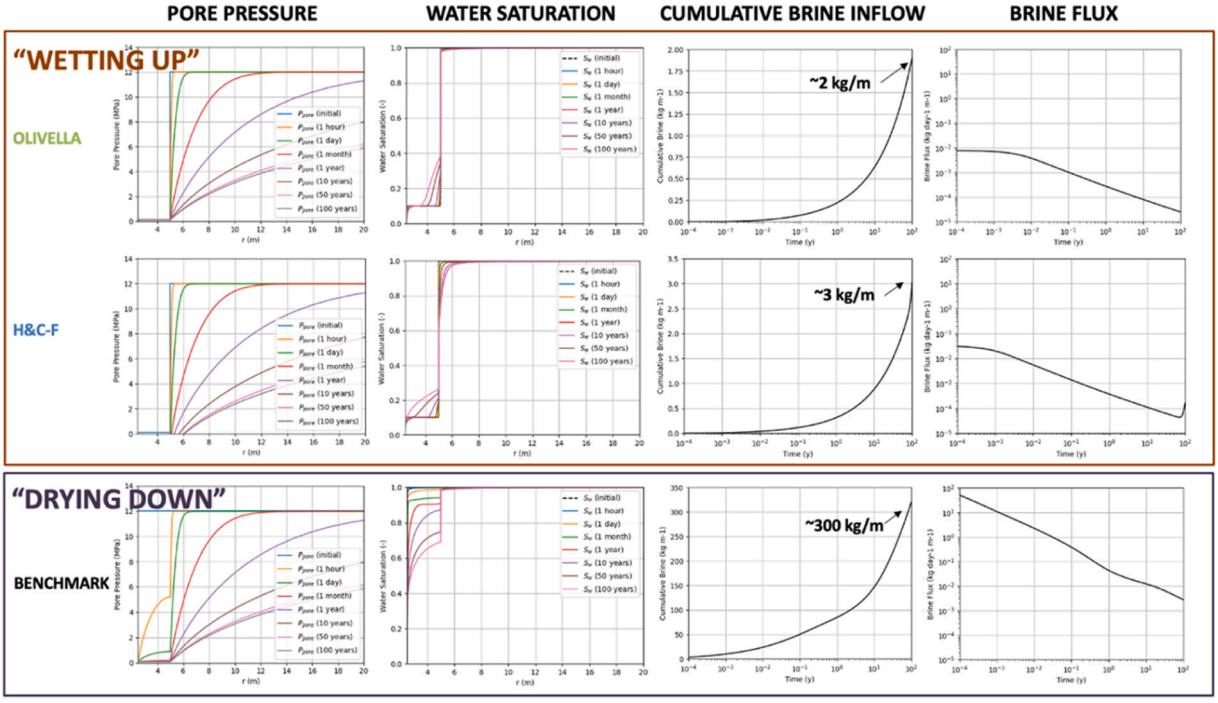

Fig. 19. Step 1b: Comparison of pore pressure, saturation, and brine inflow predictions (columns) for two different Quintessa H^2 model initializations (rows); a "wetting up" (top), and "drying down" (bottom). The curves in the left two columns of subplots show radial pressure and saturation profiles at different times (from 1 h to 100 years). The right two columns of subplots show cumulative inflow and flux to the borehole through time.

Table 4
Step 2: Team-specific configurations for BATS 1a heated brine production.

Team	Dim.	Drift EDZ	Borehole EDZ	Mechanical System	Perm.*
Quintessa/ NWS	1D	No	Assigned	Hou-Lux viscoplastic + simple damage model	$k(\epsilon, D, r)$
LANL	2D/ 3D	No	Assigned	Elastic (3D only)	$k(T)$& $k(\epsilon)$
LBNL	2D	Computed	Computed	Lux-Wolters viscoplastic w/ damage	$k(\epsilon, \sigma', P)$
BGR	2D	No	Assigned	Salt + single fracture mechanical model	$k(\sigma_3)$
SNL	3D	Assigned	Assigned	No	$k(r, T)$

* Permeability (k) was included as a function of the effective stress (σ'), pore fluid pressure (P), least principal stress (σ_3), strain (ϵ), damage (D), radial distance (r), and temperature (T)

borehole and the drift, and the relative orientation of gravity perpendicular to the HP borehole, there were necessary trade-offs in geometrical fidelity and model run-time. Several teams decided a lower-dimensional approximation was sufficient.

Quintessa and LBNL included the most physically comprehensive mechanical models and included coupling between the mechanical deformation and hydrologic parameters (i.e., ϕ, k, and Biot's coefficient), with the other teams choosing a more phenomenological approach (e.g., k reacting to temperature changes directly or using an elastic-only model). BGR used an empirical permeability model with respect to the tensile strength.

6.1. Brine production time series results

The time series of brine inflow to the heated HP borehole and corresponding model predictions through the 28 days of heating and the first three weeks of cool-down after heating are shown in Fig. 21. The early time brine production data (<6 days) are higher than the data later during the heating period due to a higher N_2 circulation flowrate.[36] Most models were not able to, or chose not to, include this difference (LANL 2D and 3D models did include this). Most of the models did a good job fitting the late-time (>14 days) brine production during heating, except the two 3D models (SNL and LANL). All except the SNL model re-created the peak in brine production at the end of heating, with the largest difference between the models during the cool-down period. The SNL model did not have an explicit mechanical component.

The initial post-heating brine production response was matched by several teams, but the extended nature of the brine production seemed anomalous, rather than an exponential decay. The BGR results show a long period of elevated brine production after heating.

6.2. Pressure and saturation profile results

While there were no observations of brine pressure or saturation made during the BATS 1a field test, the predictions of these quantities help illustrate some of the differences between the models used to predict brine inflow.

Fig. 22 shows that most of the models (except SNL) predicted a very steep boundary between partially and fully liquid saturated (note logarithmic distance scale). LANL did not produce profiles of brine saturation.

Most of the models were fully brine-saturated within 20 cm of the origin (i.e., the borehole center). The SNL model also included the drift EDZ, which in general resulted in much lower saturations (the SNL radial profile shown is perpendicular to the drift, extending from the end of the HP borehole). In the brine saturation and pressure figures, results are shown at 28 (solid) and 29 (dashed) days, which correspond to the end of heating and after 1 day of cooling.

The somewhat jagged SNL results are due to extracting results along a straight line extending away from the heated borehole from an irregular Voronoi mesh. These results occur when jumping between elements along a line that does not necessarily go through the element centers. The results are constant across each element and were not smoothed.

Fig. 23 shows profiles of formation fluid pressure going away from the borehole. Negative liquid pressures in the BGR model, is indicative of less-than-fully saturated conditions. In other models, the maximum pressure is reported, which is the liquid pressure when fully liquid saturated and the gas pressure when partially liquid saturated.

While many of the teams had 10 to 12 MPa formation pressure in the

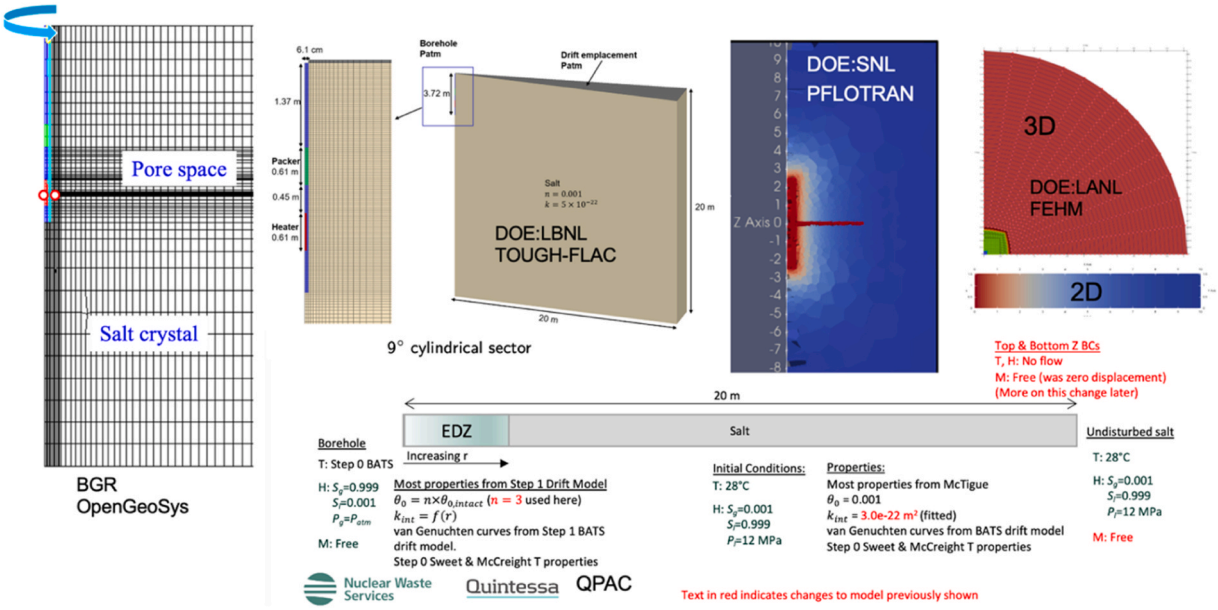

Fig. 20. Step 2: Conceptual models for the BATS 1a heated brine production step.

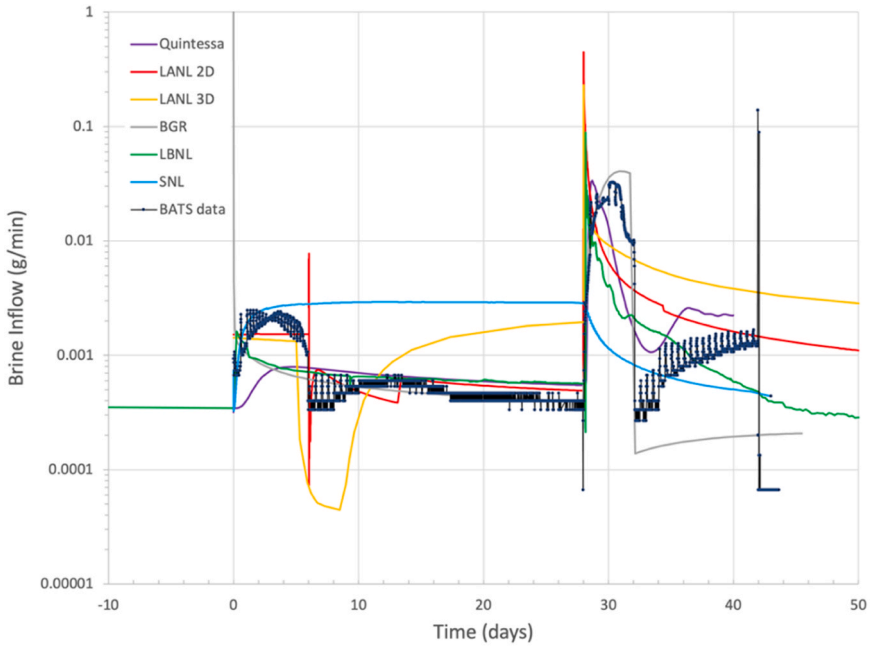

Fig. 21. Step 2: BATS 1a brine inflow data observed at HP borehole through time (dark blue line with small circular symbols) compared to model predictions (colored lines without symbols).

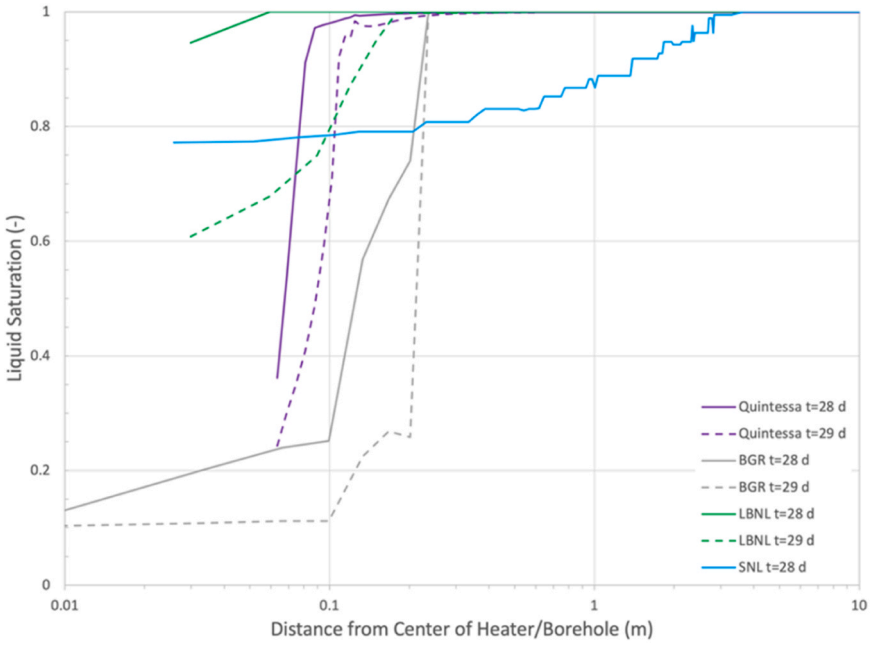

Fig. 22. Step 2: Predictions of liquid saturation with radial distance from the heater at the end of heating (28 days), and after 1 day of cooling (29 days). Line color indicates team, solid lines at end of heating, dashed lines after 1 day of cooling.

far-field (Fig. 23), the LBNL model had a lower far-field pressure. The LBNL model also developed the EDZ associated with the drift and boreholes by excavating the room and boreholes and allowing the damage to develop via the constitutive laws already implemented, rather than assigning the extent of this damage region a priori.

6.3. Permeability distributions

Fig. 24 shows the permeability variation in the models at the end of heating, and after one day of cooling for most of the teams. The LBNL and Quintessa brine inflow results are similar (Fig. 21), despite the permeability (Fig. 24) and pressure (Fig. 23) near the borehole being different. The Quintessa k after one day of cooling is higher closest to the borehole (LBNL had $k = 10^{-17}$ m^2 near the heater) but drops to a lower value with increasing distance. The LBNL unheated k (before the effects of heating and cooling, but after the effects of damage associated with construction of the borehole) is computed from constitutive relationships, while the Quintessa model uses the observations of Stormont et al.[50] to impose an EDZ with thickness equal to one borehole radius and k increasing by four orders of magnitude across the EDZ towards the borehole, with the intact salt k and EDZ ϕ constrained by the initial pre-test brine inflow observations (i.e., the 300 days before testing after

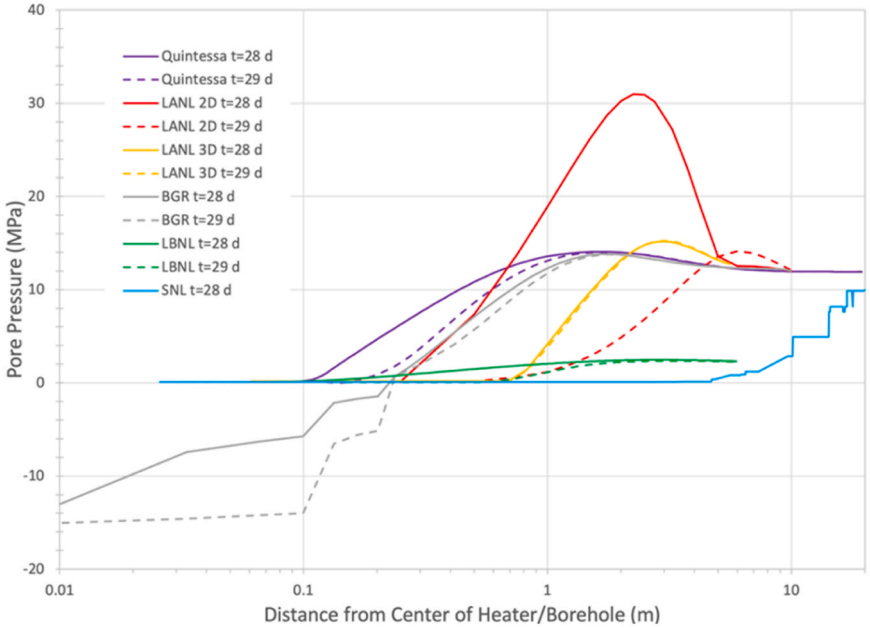

Fig. 23. Step 2: Formation fluid pressure model predictions extending radially away from heater at the end of heating (28 days, solid) and after 1 day of cooling (29 days, dashed). Line color indicates team, solid lines at end of heating, dashed lines after 1 day of cooling.

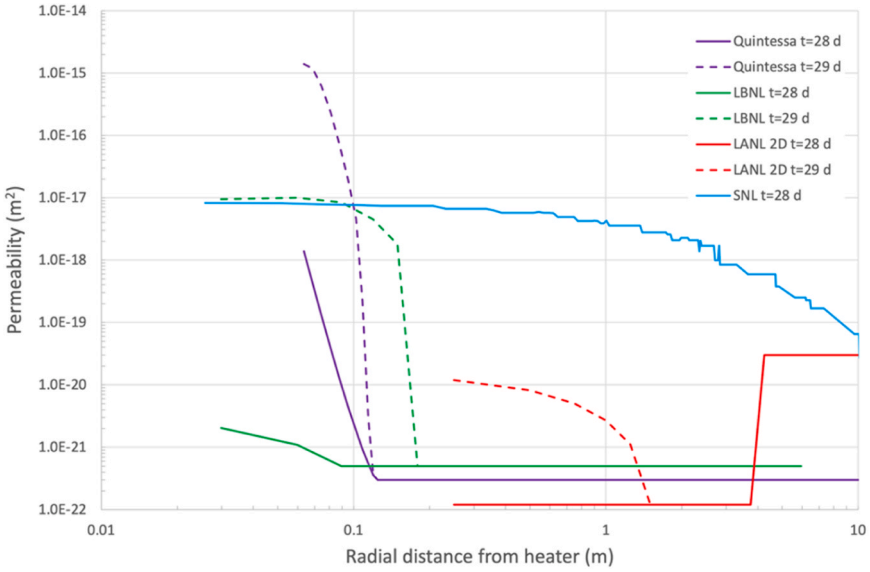

Fig. 24. Step 2: Comparison of permeability distributions at the end of heating (28 day) and after 1 day of cooling (29 day). Line color indicates team, solid lines at end of heating, dashed lines after 1 day of cooling.

the borehole was drilled).

Aside from the similarity that permeability is higher near the borehole, and lower further away, there are significant differences between the approaches taken by the teams, reflecting the different mechanisms and conceptual models used to represent the BATS 1a heater test. The LANL 2D k model (Fig. 24) included both a decrease in k near the borehole, due to thermal expansion, and an increase in k due to tensile failure of salt once cooling begins (i.e., opening fractures that were closed by thermal expansion due to heating).

The plots of permeability at different times are due to different mechanisms. Quintessa and LBNL changed k due to mechanistic changes in ϕ derived from volumetric strain and damage, while LANL changed k in relation to stress or temperature. SNL had an anisotropic k and ϕ distribution around the drifts and boreholes that changed with radial distance to excavations. The BGR model included mechanical effects (as a function of time, rather than distance), but with k of the EDZ surrounding the borehole in the flow model increasing to allow more brine into the borehole at the end of heating.

7. Summary and conclusions

Task E of DECOVALEX-2023 has gradually built-up complexity to the relevant TH^{2}M BATS 1a test. Starting from single-process benchmarks in step 0 (T and H^1), adding coupled processes and two-phase flow in step 1 (TH^{1}M and H^2). One of the most interesting aspects of this process is how each individual team approached a particular problem by implementing different initial conditions and boundary conditions, even when modeling simpler benchmarks or uncoupled processes. The Room D

benchmark (step 0a) contained multiple boreholes and demonstrated the relative importance of lithologic heterogeneity. The borehole-derived EDZ may be more important to capture for the BATS array, which has several boreholes near one another, contributing to a larger aggregate EDZ. The McTigue[40] benchmark (step 1a) demonstrated the importance of simulating the confined thermal expansion (both brine and salt) on pore pressure in heated salt formations. Finally, the variety of results from the multiphase modeling exercise (step 1d), despite its prescriptive nature, showed the simulators can produce a wide range of saturation, liquid pressure, and brine production estimates, given differences in implementation, constitutive laws, meshing, and time stepping between models. This demonstrates the complexity of multiphase flow modeling and hence the potential difficulties in relying on only a single model for the analysis of a system.

The multiphase comparison (step 1b) challenged the default hydrological modeling assumption of a "drying down" system, despite not having an analytical solution or field data to benchmark against. The "wetting up" conceptualization was agreed to be more physically realistic, and this has significant impact on brine production simulations at early time; this is likely the most relevant detail from this task to performance assessment type simulations as well. By working collaboratively to understand how each team approaches and implements numerical representations of TH^2MC simulations, teams learn from one another and expand the baseline understanding of coupled processes for heat-generating waste in salt repository science.

Step 2 of Task E focused on coupled processes observed in the BATS 1a heater test.[35] Teams matched brine production during and after heating, which includes relevant coupled physics that were discussed independently in steps 0 and 1. The thermal response was simulated in step 0a, thermal expansion was simulated in step 1a, and the effects of two-phase flow were simulated in step 1b. Step 2 involved a combination of these individual steps already considered, along with the additional consideration of hydro-mechanical feedback (e.g., thermal expansion leading to closure of ϕ and reduction of k during heating, and subsequent reversal of this process during after-test cooling).

The complexity of the BATS 1a observations forced teams to pick which aspect of the data they thought were worth focusing on. Early data showed impacts from higher gas flowrates, and data later during cooling showed extended brine production that did not follow an exponential decay. The complexities in the data, and the diversity of approaches shows there are different ways to represent the processes, but there were several common themes:

1) Permeability is higher near the borehole/excavation, to represent effects of damage.
2) Fluid pressure is highest at the end of heating, due to thermal pressurization.
3) Permeability rises at the end of heating, which allows the higher pressures to dissipate.

Future BATS testing for DECOVALEX efforts would benefit from having field test replicate experiments (to better separate the important experimental aspects from those that are more incidental), and additional laboratory testing of relevant salt samples to constrain some of the more uncertain TH^2M material parameters like two phase flow properties, thermal expansion coefficient, and Biot coefficient. Future testing should characterize the fracture network within the salt and quantify this network's two-phase and poromechanical flow properties, possibly with non-reactive pore fluids. Thermal and thermal-mechanical properties (e.g., thermal conductivity, heat capacity, thermal expansion) are easier to quantify, and can have a significant impact on results, because the problem is essentially thermally driven.

In general, the Task E exercise led to an increased understanding of the complex processes expected to occur in the EDZ of a salt repository for disposal of heat-generating radioactive waste. In the longer term (tens to hundreds of years), it is expected the drift and the damage (i.e., ϕ and k) of the EDZ will creep shut and the dynamic processes observed in BATS will be less important. Understanding these early-time and short-distance processes is important to quantify the initial conditions that performance assessment models will need, including the effects of model initialization and the amount of brine expected to flow into the drifts, as radionuclides dissolved in brine would typically be the primary release pathway. Understanding processes going on in the near field and short term are also important if any future repository design is to be optimized.

The organization of Task E tried to strike a balance between being prescriptive, which might result in more comparable outputs, and allowing complete freedom, which may better explore the possible space of modeling approaches as a group. The task details and goals were significantly refined during the four years of DECOVALEX-2023. Discussions between the task lead and the teams were a critical part of the learning as a group (i.e., between the teams), as different approaches were attempted, modified, and sometimes dropped.

The benefits from the Task E exercise extend beyond the improved conceptual understanding derived from modeling and the interactions between the teams, it also extends to the experiment design and execution. The second phase of BATS is underway,[37] and has been collecting additional data to use in follow-on phases of DECOVALEX.

CRediT authorship contribution statement

Hua Shao: Writing – original draft, Formal analysis. **Jonny Rutqvist:** Writing – original draft, Formal analysis. **Hafssa Tounsi:** Writing – original draft, Formal analysis. **Jeroen Bartol:** Writing – original draft, Formal analysis. **Philip H. Stauffer:** Writing – original draft, Formal analysis. **Kristopher L. Kuhlman:** Writing – review & editing, Writing – original draft, Supervision, Conceptualization. **Michelle Bourret:** Writing – original draft, Formal analysis. **Claire Watson:** Writing – original draft, Formal analysis. **Steven J. Benbow:** Writing – original draft, Formal analysis. **Eric Guiltinan:** Writing – original draft, Formal analysis. **Oliver Czaikowski:** Writing – original draft, Formal analysis. **Kyra Jantschik:** Writing – original draft, Formal analysis. **Simon Norris:** Writing – original draft, Formal analysis. **Richard Jayne:** Writing – original draft, Formal analysis.

Declaration of Competing Interest

The authors declare that they have no known competing financial interests or personal relationships that could have appeared to influence the work reported in this paper.

Data Availability

Data will be made available on request.

Acknowledgements

DECOVALEX is an international research project comprising participants from industry, government and academia, focusing on development of understanding, models and codes in complex coupled problems in sub-surface geological and engineering applications; DECOVALEX-2023 is the current phase of the project. The authors appreciate and thank the DECOVALEX-2023 Funding Organisations Andra, BASE, BGE, BGR, CAS, CNSC, COVRA, US DOE, ENRESA, ENSI, JAEA, KAERI, NWMO, NWS, SÚRAO, SSM and Taipower for their financial and technical support of the work described in this paper. The statements made in the paper are, however, solely those of the authors and do not necessarily reflect those of the Funding Organisations.

This paper describes objective technical results and analysis. Any subjective views or opinions that might be expressed in the paper do not necessarily represent the views of the U.S. Department of Energy or the United States Government.

The U.S. co-authors of this work were funded by the U.S. Department of Energy Office of Nuclear Energy's Spent Fuel and Waste Science and Technology Campaign.

References

1. Beauheim RL, Roberts RM. Hydrology and hydraulic properties of a bedded evaporite formation. *J Hydrol.* 2002;259:66–88.
2. Beauheim, R.L., A. Ait-Chalel , G. Vouille, et al. , 1997. INTRAVAL Phase 2 WIPP 1 Test Case Report: Modeling of Brine Flow Through Halite at the Waste Isolation Pilot Plant Site, (124 p.) SAND97–0788. Albuquerque, NM: Sandia National Laboratories. ⟨https://doi.org/10.2172/481481⟩.
3. Benbow, S., C. Watson, A. Bond, S. Norris & S. Parsons, 2022. "Near-Field Coupled Processes in Salt-Based Disposal Facilities – Learning from Modelling in DECOVALEX-2023″ in International High-Level Radioactive Waste Management Conference, Phoenix AZ, 13–17 November 2022.
4. Benbow S, Watson C, Bond A, Norris S, Parsons S, Kuhlman KL. Coupled modelling of brine availability in salt-based disposal facilities - learning from DECOVALEX 2023, in powering the energy transition through subsurface collaboration. *Br Geol Soc.* 2024.
5. Bond A, Birkholzer JT. DECOVALEX-2023 - an international collaboration on modeling of coupled subsurface processes important for radioactive waste disposal. *Geomech Energy Environ.* 2024.
6. Cinar Y, Pusch G, Reitenbach V. Petrophysical and capillary properties of compacted salt. *Transp Porous Media.* 2006;64(2):199–228.
7. COMSOL Inc., COMSOL Multiphysics Reference Manual, (1742 p.) version 5.5, Stockholm, Sweden, 2019.
8. Dai Z, Xu L, Xiao T, et al. Reactive chemical transport simulations of geologic carbon sequestration: methods and applications. *Earth-Sci Rev.* 2020;208, 103265.
9. David C, Wong T-F, Zhu W, Zhang J. Laboratory measurement of compaction-induced permeability change in porous rocks: implications for the generation and maintenance of pore pressure excess in the crust. *Pure Appl Geophys.* 1994;143(13):425–456.
10. Davies, C. & F. Bernier, Impact of the Excavation Disturbed or Damaged Zone (EDZ) on the Performance of Radioactive Waste Geologic Repositories, (359 p.) EUR 21028 EN. Luxembourg: European Commission Nuclear Science and Technology, 2005.
11. Davies, P.B., Evaluation of the Role of Threshold Pressure in Controlling Flow of Waste-Generated Gas into Bedded Salt at the Waste Isolation Pilot Plant, (62 p.) SAND90–3246. Albuquerque, NM: Sandia National Laboratories, 1991. https://doi.org/10.2172/5578858.
12. Finley, S.J., D.J. Hanson & R. Parsons, Small-Scale Brine Inflow Experiments – Data Report Through 6/6/91, (185 p.) SAND91–1956. Albuquerque, NM: Sandia National Laboratories, 1992.
13. Freeze, G.A., T.L. Christian-Frear & S.W. Webb, 1997. Modeling Brine Inflow to Room Q: A Numerical Investigation of Flow Mechanisms, (117 p.) SAND96–0561, Sandia National Laboratories, Albuquerque, NM. ⟨https://doi.org/10.2172/481483⟩.
14. Guiltinan EJ, Kuhlman KL, Rutqvist J, et al. Temperature response and brine availability to heated boreholes in bedded salt. *Vadose Zone J.* 2020;19(1), e20019.
15. Guiltinan, E. , J. Bartol , S. Benbow, et al., Brine Availability Test in Salt: Collaborative Modeling within DECOVALEX in International High-level Radioactive Waste Management Conference, Phoenix AZ, 13–17, 2022b.
16. Guiltinan, E. , J. Bartol , S. Benbow, et al., Brine Availability Test in Salt: International Collaborative Modeling in the DECOVALEX Project – 22164″ in waste management symposium, Phoenix AZ, 6–10, 2022a.
17. Hammond GE, Lichtner PC, Mills RT. Evaluating the performance of parallel subsurface simulators: an illustrative example with PFLOTRAN. *Water Resour Res.* 2014;50(1):208–228.
18. Hansen, F.D., 2003. The Disturbed Rock Zone at the Waste Isolation Pilot Plant, (62 p.) SAND2003–3407. Albuquerque, NM: Sandia National Laboratories. ⟨https://doi.org/10.2172/918258⟩.
19. Hansen F, Popp T, Wieczorek K, Stuehrenberg D. Granular salt summary: reconsolidation principles and applications, (82 p.) SAND2014–16141R. *Albuq, NM: Sandia Natl Lab*; 2014. ⟨https://doi.org/10.2172/1164616⟩.
20. Hohlfelder, J.J., 1979. Salt Block II: Description and Results, (62 p.) SAND79–2226. Albuquerque, NM: Sandia National Laboratories. ⟨https://doi.org/10.2172/5277822⟩.
21. Howarth, S.M. & T. Christian-Frear, 1997. Porosity, Single-Phase Permeability, and Capillary Pressure Data from Preliminary Laboratory Experiments on Selected Samples from Marker Bed 139 at the Waste Isolation Pilot Plant, (3 vol.) SAND94–0472. Albuquerque, NM: Sandia National Laboratories. ⟨https://doi.org/10.2172/527912⟩.
22. Hudson JA, Stephansson O, Andersson J, Tsang CF, Jing L. Coupled T–H–M issues relating to radioactive waste repository design and performance. *Int J Rock Mech Min Sci.* 2001;38(1):143–161.
23. Itasca, 2021. *Fast Lagrangian Analysis of Continua (FLAC3D) Program Guide*, Version 7.0, Minneapolis, MN: Itasca Consulting, Inc.
24. Jayne RS, Kuhlman KL. Utilizing temperature and brine inflow measurements to constrain reservoir parameters during a salt heater test. *Minerals.* 2020;10(11):1025.
25. Jayne RS, Kuhlman KL. Utilizing high-resolution 3D Voronoi meshing to analyze field data from the Brine Availability Test in Salt (BATS). *Geomech Energy Environ.* 2024.
26. Johnson PJ, Otto S, Weaver DJ, et al. Heat-generating nuclear waste in salt: field testing and simulation. *Vadose Zone J.* 2019;18(1):1–14.
27. Johnson PJ, Zyvoloski GA, Stauffer PH. Impact of a porosity-dependent retention function on simulations of porous flow. *Transp Porous Media.* 2019;127(1):211–232.
28. Jordan AB, Boukhalfa H, Caporuscio FA, Robinson BA, Stauffer PH. Hydrous mineral dehydration around heat-generating nuclear waste in bedded salt formations. *Environ Sci Technol.* 2015;49(11):6783–6790.
29. Jung Y, Pau GSH, Finsterle S, Doughty C. *TOUGH3 User's Guide*. LBNL-2001093. Berkeley, CA: Lawrence Berkeley National Laboratory,; 2018:170. https://doi.org/10.2172/1461175.
30. Kolditz O, Görke U-J, Shao H, Wang W. *Thermo-Hydro-Mechanical-Chemical Processes in Porous Media - Benchmarks and Examples*. vol. 86. Springer,; 2012.
31. Kuhlman, K.L., 2014. Summary Results for Brine Migration Modeling Performed by LANL, LBNL, and SNL for the UFD Program, (105 p.) SAND2014–18217R. Albuquerque, NM: Sandia National Laboratories. ⟨https://doi.org/10.2172/1163122⟩.
32. Kuhlman, K.L., 2019. Processes in Salt Repositories, (41 p.) SAND2019–6441R. Albuquerque, NM: Sandia National Laboratories. ⟨https://doi.org/10.2172/1559569⟩.
33. Kuhlman, K.L., 2020. DECOVALEX-2023 Task E Specification Revision 0, (32 p.) SAND2020–4289R. Albuquerque, NM: Sandia National Laboratories. ⟨https://doi.org/10.2172/1616375⟩.
34. Kuhlman KL. *DECOVALEX-2023 Task E final report*. Berkeley, CA: Lawrence Berkeley National Laboratory,; 2023.
35. Kuhlman, K., M. Mills , R. Jayne, et al. , 2021. Brine Availability Test in Salt (BATS) FY21 Update, (64 p.) SAND2021–10962R. Albuquerque, NM: Sandia National Laboratories. ⟨https://doi.org/10.2172/1821547⟩.
36. Kuhlman, K., M. Mills, R. Jayne, et al. , 2020. FY20 Update on Brine Availability Test in Salt, (107 p.) SAND2020–9034R. Albuquerque, NM: Sandia National Laboratories. ⟨https://doi.org/10.2172/1657890⟩.
37. Kuhlman, K., M. Mills, R. Jayne, et al. , 2023. Brine Availability Test in Salt (BATS) FY23 Update, (88 p.) SAND2023–08820R. Albuquerque, NM: Sandia National Laboratories. https://doi.org/10.2172/2369628.
38. LaForce T, Bartol J, Becker D-A, et al. Comparing modelling approaches for a generic nuclear waste repository in salt. *Geomech Energy Environ.* 2024.
39. McTigue DF. Thermoelastic response of fluid-saturated porous rock. *J Geophys Res.* 1986;91(B9):9533–9542.
40. McTigue DF. Flow to a heated borehole in porous, thermoelastic rock: analysis. *Water Resour Res.* 1990;26(8):1763–1774.
41. McTigue, D.F., 1993. Permeability and Hydraulic Diffusivity of Waste Isolation Pilot Plan Repository Salt Inferred from Small-Scale Brine Inflow Experiments, (91 p.) SAND92–1911. Albuquerque, NM: Sandia National Laboratories. Please add DOI for this report: https://doi.org/10.2172/10114964.
42. Olivella S, Castagana S, Alonso EE, Lloret A. Porosity variations in saline media induced by temperature gradients: experimental evidences and modelling. *Transp Porous Media.* 2011;90(3):763–777.
43. Olivella S, Vaunat J, Rodriguez-Dono A. *CODE_BRIGHT User's Guide*. Barcelona, Spain: Universitat Politècnica de Catalunya,; 2021:226.
44. Pandey SN, Vishal V, Chaudhuri A. Geothermal reservoir modeling in a coupled thermo-hydro-mechanical-chemical approach: a review. *Earth-sci Rev.* 2018;185:1157–1169.
45. Popp T, Kern H, Schulze O. Evolution of dilatancy and permeability in rock salt during hydrostatic compaction and triaxial deformation. *J Geophys Res.* 2001;106(B3):4061–4078.
46. Quintessa, 2013. *QPAC:* Quintessa's General-Purpose Modelling Software. Quintessa Report QRS-QPAC-11 (⟨http://www.quintessa.org/qpac-overview-report.pdf⟩). Henley-on-Thames, UK: Quintessa Limited.
47. Rutqvist J. Status of the TOUGH-FLAC simulator and recent applications to coupled fluid flow and crustal deformations. *Comput Geosci.* 2011;37(6):739–750.
48. Shao H, Hesser J, Wang W, Kolditz O. Modeling thermally driven migration of brine in bedded salt. *Geomech Energy Environ.* 2024;38, 100542. https://doi.org/10.1016/j.gete.2024.100542.
49. Stauffer, P.H. , K. Kuhlman , J. Rutqvist, et al., 2020, 2020 Update on the US DOE Generic Salt Repository URL - Brine Availability Test in Salt – 21152, Waste Management Symposium, March 8–12, 2020, Phoenix AZ. LA-UR-21–20548.
50. Stormont, J.C., C.L. Howard & J.J.K. Daemen, 1991. In Situ Measurements of Rock Salt Permeability Changes Due to Nearby Excavations, (81 p.) SAND90–3134. Albuquerque, NM: Sandia National Laboratories. ⟨https://doi.org/10.2172/6244387⟩.
51. Sweet, J.N. & J.E. McCreight, 1980. Thermal Properties Measurement on Rocksalt Samples from the Site of the Proposed Waste Isolation Pilot Plant, (79 p.) SAND80–709. Albuquerque, NM: Sandia National Laboratories. ⟨https://doi.org/10.2172/5510643⟩.

52. Tounsi, H., J. Rutqvist, M. Hu & K. Kuhlman, 2022. "THM Modeling of Brine Migration in A Heated Borehole Test in Bedded Salt" in 3rd International Conference on Coupled Processes in Fractured Geological Media: Observation, Modeling, and Application (CouFrac2022), Berkeley, CA, 14–16 November 2022.
53. Tounsi H, Rutqvist J, Hu M, Kuhlman K. Thermo-hydro-mechanical modeling of brine migration in a heated borehole test in bedded salt. *Rock Mech Rock Engine*. 2023.
54. Tounsi H, Rutqvist J, Hu M, Wolters R. Numerical investigation of heating and cooling-induced damage and brine migration in geologic rock salt: insights from coupled THM modeling of a controlled block scale experiment. *Comput Geotech*. 2023;154, 105611.
55. Tsang CF. *Coupled processes associated with nuclear waste repositories*. Elsevier,; 2012.
56. van Genuchten MTh. A closed-form equation for predicting the hydraulic conductivity of unsaturated soils. *Soil Sci Soc Am J*. 1980;44(5):892–898.
57. Wang J, Uhlemann S, Otto S, Dozier B, Kuhlman K, Wu Y. Joint geophysical and numerical insights of the coupled thermal-hydro-mechanical processes during heating in salt. *J Geophys Res Solid Earth*. 2023;128(9).
58. Watson C, Benbow S, Bond A, Norris S, Parsons S. A simple model to represent damage and fracturing in rock salt caused by heating and subsequent cooling: understanding brine inflow data from the Brine Availability Test in Salt (BATS). *Geomech Energy Environ*. 2024.
59. Webb, S.W., 1992. Brine Inflow Sensitivity Study for Waste Isolation Pilot Plant Boreholes: Results of One-Dimensional Simulations, (234 p.) SAND91–2296. Albuquerque, NM: Sandia National Laboratories.
60. Zivar D, Kumar S, Foroozesh J. Underground hydrogen storage: a comprehensive review. *Int J Hydrog Energy*. 2021;46(45):23436–23462.
61. Zyvoloski GA, Robinson BA, Dash ZV, et al. *Software User's Manual (UM) for the FEHM Application Version 3.1-3.X*. Los Alamos, NM: Los Alamos National Laboratory,; 2015:329.